

ANALYSIS OF NARCISSUS EFFECT IN INFRARED OPTICAL SYSTEMS  
WITH COOLED DETECTORS

A THESIS SUBMITTED TO  
THE GRADUATE SCHOOL OF NATURAL AND APPLIED SCIENCES  
OF  
MIDDLE EAST TECHNICAL UNIVERSITY

BY

SERHAT HASAN ASLAN

IN PARTIAL FULFILLMENT OF THE REQUIREMENTS  
FOR  
THE DEGREE OF DOCTOR OF PHILOSOPHY  
IN  
PHYSICS

JULY 2022



Approval of the thesis:

**ANALYSIS OF NARCISSUS EFFECT IN INFRARED OPTICAL SYSTEMS  
WITH COOLED DETECTORS**

submitted by **SERHAT HASAN ASLAN** in partial fulfillment of the requirements  
for the degree of **Doctor of Philosophy in Physics Department, Middle East  
Technical University** by,

Prof. Dr. Halil Kalıpçılar  
Dean, Graduate School of **Natural and Applied Sciences**

\_\_\_\_\_

Prof. Dr. Seçkin Kürkçüoğlu  
Head of Department, **Physics**

\_\_\_\_\_

Assoc. Prof. Dr. Sinan Kaan Yerli  
Supervisor, **Physics Department, METU**

\_\_\_\_\_

**Examining Committee Members:**

Assoc. Prof. Dr. Özlem Duyar Coşkun  
Physics Engineering Department, Hacettepe University

\_\_\_\_\_

Assoc. Prof. Dr. Sinan Kaan Yerli  
Physics Department, METU

\_\_\_\_\_

Assoc. Prof. Dr. Alpan Bek  
Physics Department, METU

\_\_\_\_\_

Prof. Dr. Hakan Altan  
Physics Department, METU

\_\_\_\_\_

Prof. Dr. Akın Bacıoğlu  
Physics Engineering Department, Hacettepe University

\_\_\_\_\_

Date:

**I hereby declare that all information in this document has been obtained and presented in accordance with academic rules and ethical conduct. I also declare that, as required by these rules and conduct, I have fully cited and referenced all material and results that are not original to this work.**

**In collaboration with my supervisor the following research article has been published:**

*Thin lens narcissus model in infrared lens design with cooled detectors,*

**S.H.Aslan and S.K.Yerli, , Appl. Opt., vol. 61, no. 3, pp. 728–736, Jan 2022.**

**The main contributor of this work is myself and Assoc. Prof. Dr. Sinan Kaan YERLİ helped me to structure the work into research article. This article is extended and taken as a base in my thesis.**

Name, Surname: Serhat Hasan Aslan

Signature :

## **ABSTRACT**

### **ANALYSIS OF NARCISSUS EFFECT IN INFRARED OPTICAL SYSTEMS WITH COOLED DETECTORS**

Aslan, Serhat Hasan

Ph.D., Department of Physics

Supervisor: Assoc. Prof. Dr. Sinan Kaan Yerli

July 2022, 90 pages

Infrared lens design has many aspects similar to visible lens design. Optical aberration types and calculations, tolerancing procedures are applied in the same way in infrared lens design as in the visible lens design. However, there are many design aspects in infrared lens which are very different from visible lens design. One of these aspects is the narcissus effect in infrared lenses utilizing cooled infrared detectors. Narcissus effect is a very well known phenomenon in infrared lens with cooled detectors designed for high performance military electro-optical systems. It is the retroreflection of the cooled detector onto itself from refractive lens surfaces and seen as a dark spot at the center of the infrared image. It highly degrades the quality of the infrared image if it is not controlled in infrared lens design stages. Narcissus is controlled by two very important paraxial parameters in infrared lens design. While one of these paraxial parameters control the amplitude of the narcissus distribution, the other controls the variation of the narcissus distribution across the detector. Narcissus performance of an infrared lens is generally analysed at the far end of the optical lens design at which the main architecture of the optical layout, lens numbers and materials are already determined. If the narcissus performance of the designed lens

is not satisfactory, very time consuming and inefficient iterations are needed in order to achieve a satisfactory optical performance from both optical aberrations and narcissus perspective. In this thesis, a narcissus control technique which enables optical designers to control narcissus effect in the early stages of the infrared lens design is constructed. Conventional paraxial narcissus control parameters are transformed into two narcissus control metrics which are used as a new type of aberration similar to the Seidel aberration coefficients. Narcissus performance of a lens can be taken into consideration in the early design stages beside optical aberrations with the help of the proposed thin lens narcissus model.

**Keywords:** infrared lens design, optical aberrations, narcissus effect, cooled infrared detectors

## ÖZ

### SOĞUTMALI DEDEKTÖRLÜ KIZILÖTESİ GÖRÜNTÜLEME SİSTEMLERİNDE NARSİS ANALİZİ

Aslan, Serhat Hasan

Doktora, Fizik Bölümü

Tez Yöneticisi: Doç. Dr. Sinan Kaan Yerli

Temmuz 2022, 90 sayfa

Kızılötesi lens tasarımı görünür bölge lens tasarımıyla birçok yönden benzerlik gösterir. Optik bozulum tipleri ve hesaplamaları, toleranslandırma yöntemleri görünür bölge lenslerinde uygulandığı gibi kızılötesi lenslerde de uygulanır. Ancak, kızılötesi lenslerde görünür bölge lenslerinden çok farklı tasarım yönleri vardır. Bu yönlerden biri de soğutmalı kızılötesi dedektörlerin kullanıldığı kızılötesi lenslerde görülen narsis etkisidir. Narsis etkisi yüksek performanslı askeri elektrooptik sistemler için tasarlanan soğutmalı dedektörlü kızılötesi lenslerde bilinen bir etkidir. Bu etki, soğutmalı dedektörün kırılmalı optik lens yüzeylerinden kendi üzerine geri yansımadır ve kızılötesi görüntüde merkezde siyah bir daire olarak görülür. Narsis etkisi lens tasarım safhalarında kontrol edilmezse, kızılötesi görüntü kalitesini oldukça düşürür. Narsis etkisi kızılötesi lens tasarımında iki tane paraksial parametreyle kontrol edilir. Bu parametrelerden biri narsis dağılımının büyüklüğünü kontrol ederken, diğeri dedektör üzerindeki dağılımını kontrol eder. Narsis etkisi genelde optik mimarinin, lens sayıları ve malzemelerinin halihazırda belirlenmiş olduğu optik lens tasarımının son safhalarında analiz edilir. Eğer narsis performansı yeterli seviyede değilse, hem optik

bozulmalar hem de narsis aısından yeterli seviyeye ulařmak iin oldukça verimsiz ve zaman alan iterasyonlara ihtiya vardır. Bu tezde, optik tasarımcıların narsis etkisini erken lens tasarım safhalarında kontrol edebilmelerini saėlayan bir narsis kontrol tekniėi geliřtirilmiřtir. Geleneksel paraksiyel narsis kontrol parametreleri Seidel bozulma katsayılarına benzer yeni bir bozulma katsayısı olarak kullanılabilir iki narsis kontrol metriėine dnüşürülmüřtür. Önerilen narsis kontrol modeliyle bir lensin narsis performansı optik bozulmaların yanında lens tasarımının erken safhalarında dikkate alınabilir.

Anahtar Kelimeler: kızılötesi lens tasarımı, optik görüntü bozulmaları, narsis etkisi, soėutmalı kızılötesi dedektörler



To my family

## **ACKNOWLEDGMENTS**

I would like to thank to my supervisor Assoc. Prof. Dr. Sinan Kaan Yerli for his advice, criticism, support and encouragements throughout this work.

I am grateful to ASELSAN Electronics Industries Inc. for its all support to my studies.

Finally, it would not have been possible to write this thesis without endless support of my family: İbrahim Aslan, Çilem Aslan, Ferhat Aslan, Ebru Ataş Aslan and Bergüzar Aslan.

## TABLE OF CONTENTS

ABSTRACT . . . . .	v
ÖZ . . . . .	vii
ACKNOWLEDGMENTS . . . . .	x
TABLE OF CONTENTS . . . . .	xi
LIST OF TABLES . . . . .	xiii
LIST OF FIGURES . . . . .	xiv
LIST OF ABBREVIATIONS . . . . .	xvii
CHAPTERS	
1 INTRODUCTION . . . . .	1
1.1 Motivation and Problem Definition . . . . .	1
1.2 Proposed Methods and Models . . . . .	6
1.3 The Outline of the Thesis . . . . .	8
2 NARCISSUS EFFECT AND ITS ANALYSIS TECHNIQUES . . . . .	11
2.1 Narcissus Effect and Its Causes . . . . .	11
2.2 Narcissus Analysis and Control Techniques . . . . .	14
3 THIN LENS NARCISSUS MODEL . . . . .	27
3.1 Seidel Aberration Theory . . . . .	27
3.2 Thin Lens Narcissus Model Derivation . . . . .	34

4	APPLICATION OF THE THIN LENS NARCISSUS MODEL . . . . .	39
4.1	Specifications and Paraxial Layout . . . . .	39
4.2	Shape Factor Optimization . . . . .	44
4.3	Real Thin Lens Layout and Narcissus Performance . . . . .	46
4.4	Real Thick Lens Layout and Narcissus Performance . . . . .	49
5	CONCLUSION . . . . .	59
	REFERENCES . . . . .	61
	APPENDICES	
A	ZEMAX NARCISSUS MACRO . . . . .	65
B	FRED NARCISSUS SCRIPT . . . . .	81
	CURRICULUM VITAE . . . . .	89

## LIST OF TABLES

### TABLES

Table 1.1	Specifications of a fictitious Midwave Infrared(MWIR) lens. . . . .	4
Table 2.1	Infrared transmitting materials [1]. . . . .	12
Table 2.2	<i>y<sub>ni</sub></i> based and real-ray trace based ghost spot radius. . . . .	15
Table 3.1	Algebraic and vectorial notation of optical aberration [2]. . . . .	32
Table 4.1	Specifications of the LWIR application used in this thesis. . . . .	40
Table 4.2	Lens data of the LWIR application used in this thesis. . . . .	45
Table 4.3	Seidel coefficients of the LWIR application. . . . .	46
Table 4.4	Results of the LWIR application for the proposed narcissus model. . . . .	47
Table 4.5	Lens data of the LWIR application after transforming paraxial lenses into real lenses. . . . .	48
Table 4.6	Lens data of the LWIR application after lenses are thickened. . . . .	51

## LIST OF FIGURES

### FIGURES

Figure 1.1	Geometric view of imaging condition. . . . .	1
Figure 1.2	Systematic lens design approach [3]. . . . .	2
Figure 1.3	Optical architectures. . . . .	3
Figure 1.4	MWIR designs. . . . .	4
Figure 1.5	MTF performance of MWIR designs. . . . .	5
Figure 1.6	Narcissus performance of MWIR designs. . . . .	6
Figure 1.7	Thin lens narcissus model. . . . .	7
Figure 2.1	Infrared images with severe narcissus effects [4, 5]. . . . .	11
Figure 2.2	Narcissus spots with two different surface curvatures. . . . .	14
Figure 2.3	A typical 3 element MWIR lens. . . . .	15
Figure 2.4	A typical 4 element MWIR lens. . . . .	16
Figure 2.5	A typical vignetting plot for different $i/\bar{i}$ values. . . . .	17
Figure 2.6	Narcissus macro outputs. . . . .	20
Figure 2.7	A typical simple infrared setup for narcissus analysis in FRED platform. . . . .	23
Figure 2.8	Outputs of narcissus analysing script coded in FRED. . . . .	24

Figure 2.9	Offset corrected outputs of narcissus analysing script coded in FRED. . . . .	25
Figure 2.10	TSE outputs of narcissus analysing script coded in FRED. . . . .	26
Figure 3.1	A typical optical aberration of a real lens. . . . .	27
Figure 3.2	Aberration representations. . . . .	28
Figure 3.3	Wavefront aberration in an optical system. . . . .	29
Figure 3.4	Field and pupil vectors in an optical system. . . . .	29
Figure 3.5	Marginal ray trace. . . . .	34
Figure 4.1	Atmospheric windows in infrared [6]. . . . .	39
Figure 4.2	Optical layouts designed with computerized methods. . . . .	41
Figure 4.3	MTF and Narcissus performances of optical layouts designed with computerized methods. . . . .	42
Figure 4.4	Paraxial layout of the LWIR application. . . . .	44
Figure 4.5	Optical layout of the LWIR application with real thin lenses. . . . .	47
Figure 4.6	Optical performance and Narcissus performance of the LWIR application with real thin lenses. . . . .	50
Figure 4.7	Optical layout of the LWIR application with real thick lenses. . . . .	51
Figure 4.8	Optical performance and Narcissus performance of the LWIR application with real thick lenses. . . . .	52
Figure 4.9	FRED models of LWIR application. . . . .	54
Figure 4.10	NITD performance of LWIR application analysed by script coded in FRED scripting environment. . . . .	55

Figure 4.11	Offset NITD performance of LWIR application analysed by script coded in FRED scripting environment. . . . .	56
Figure 4.12	TSE distribution of LWIR application analysed by script coded in FRED scripting environment. . . . .	57



## LIST OF ABBREVIATIONS

MWIR	Midwave Infrared
MTF	Modulation Transfer Function
NITD	Narcissus Induced Temperature Difference
ZPL	ZEMAX Programming Language
LWIR	Longwave Infrared
OTF	Optical Transfer Function
HOT	High Operating Temperature
NARC- $\Delta T$	Narcissus in terms of Scene Temperature Difference
TSE	Thermal Self Emission
OPD	Optical Path Difference
NETD	Noise Equivalent Temperature Difference
FPA	Focal Plane Array
DLS	Damped Least Squares



## CHAPTER 1

### INTRODUCTION

#### 1.1 Motivation and Problem Definition

The main aim of an optical lens is to project each and every point in the object plane to another point in the image plane. A detector which is sensitive to the radiation emitted from the source is placed at the image plane. This imaging property of lenses could be expressed from the geometric point of view as follows: each ray or pencil emitted from a source point must meet at another point in the image plane. This geometrical principle of imaging is given in Fig. 1.1

There are many different types of starting points for a lens design. First, a mental guess could generate a suitable starting point for an experienced designer. However, results of mental guess for an inexperienced designer will be disappointing. Second, a design which is studied previously in a company will be a good starting point. Third, purchasing and analysing a competing optical system shall provide a good starting point. Fourth, a lens design database and patent file search are very beneficial in order

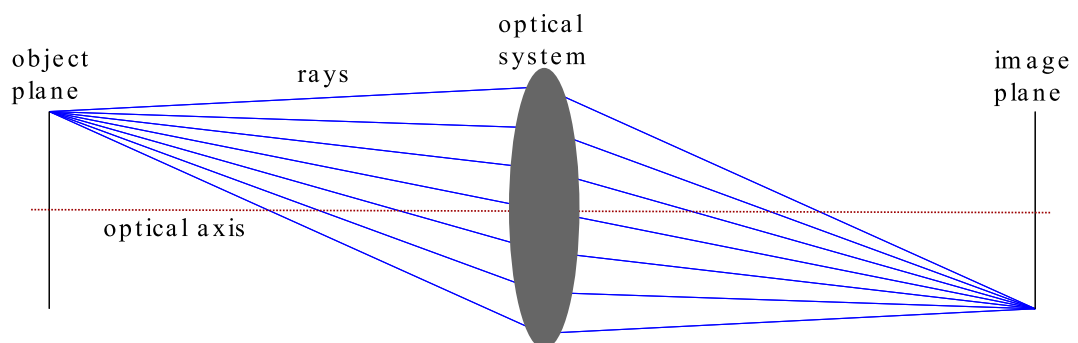


Figure 1.1: Geometric view of imaging condition.

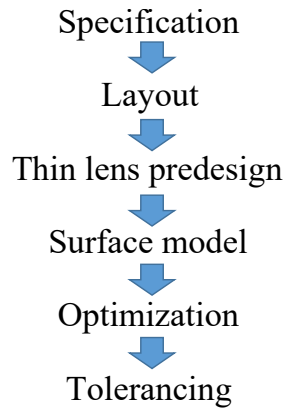


Figure 1.2: Systematic lens design approach [3].

to find a promising starting point [7]. Although these strategies are very beneficial and effective from optical design perspective, a systematic optical design approach will be used in this thesis. The flow diagram of this approach is given in Fig. 1.2 [3]. In specifications stage, optical specifications are determined and studied. After specifications are determined and studied carefully, a suitable optical architecture is chosen.

According to the optical specifications, certain types of optical architectures are well known and applied. Most of the optical systems are based on these architectures. Different types of refractive and reflective optical architectures are given in Fig. 1.3 [8]. Optical architecture defines the general optical layout which gives information about the optical power distributions and positions paraxially. At this stage, optical components are in their paraxial forms which satisfy the focal length, field of view and aperture. Once the optical layout stage is finished, optical powers, positions and materials of optical components are determined. After layout stage, thin lens pre-design stage is studied. At thin lens pre-design stage, lens shape factors are calculated according to thin lens Seidel aberration coefficients. Optical lenses can now be transformed into zero thickness real lenses from their paraxial forms. By using the surface model, thicknesses are introduced to the lenses in order them to carry optical power. At the optimization stage, optimization is done in order to improve the image quality by balancing aberrations and searching much better solutions in the design hyper-space. Finally, designed optical lens is toleranced in order to assess its statistical optical performance.

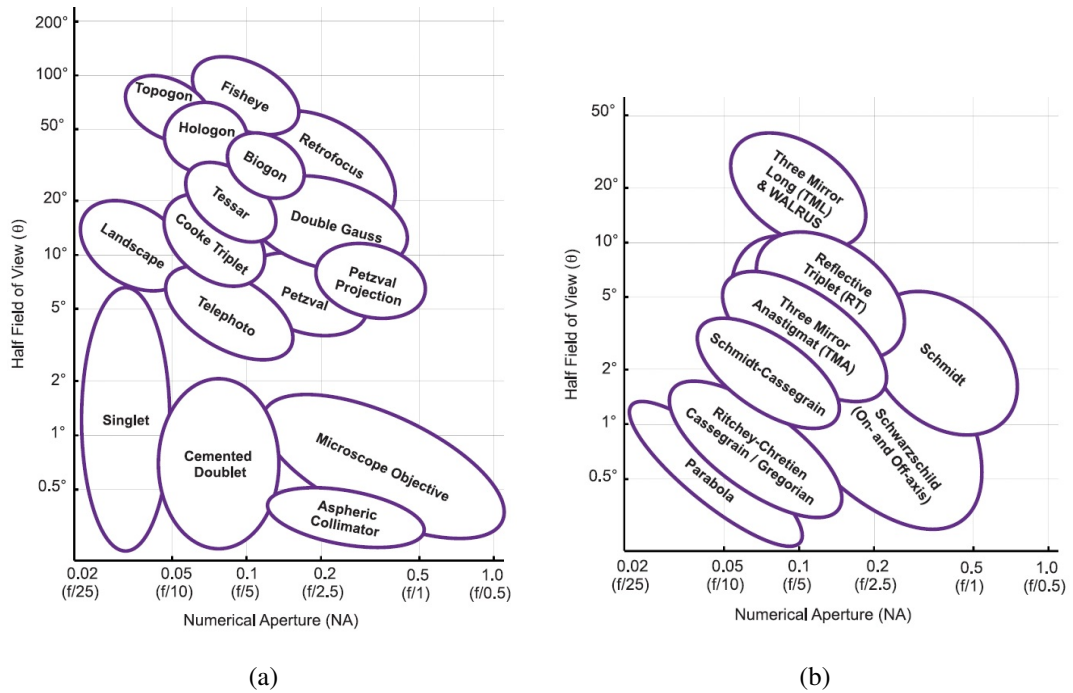


Figure 1.3: Optical architectures: (a) Refractive types, (b) Reflective types [8].

The abovementioned optical design method is common to the majority of the optical systems. However, there are many other optical phenomena which must be taken into account in optical design depending on the operating wavelength, optical materials used and operating conditions. Infrared lenses are a decent example to this situation. Although many design steps are common with visible lenses, there are many different steps that must be taken into account in infrared lens design [9]. One of the main difference is the athermalization. Since visible glasses absorb infrared radiation, they cannot be used in infrared design. Hence, different types of infrared transmitting materials such as germanium, silicon, zinc selenide, zinc sulfide, sapphire etc. are used in infrared lenses. Unfortunately, refractive indices of these infrared transmitting materials change drastically under temperature change such that the image quality is highly degraded and the optical system becomes unusable. In order to solve the defocus problem due to temperature change, athermalization effect must be included in the lens design stage. Another difference is the narcissus effect in the infrared lenses utilizing cooled detectors. Narcissus is the retro-reflection of the cold detector onto itself in infrared lenses. Narcissus effect generally shows itself as a sharp dark disk at

Table 1.1: Specifications of a fictitious Midwave Infrared(MWIR) lens.

$f_{\#}$	5.5
Detector pixels	$640 \times 512$
Detector pixel size	$15 \mu\text{m}$
Cold stop height	19.1 mm
Operating wavelength	$3.6\text{-}4.9 \mu\text{m}$
Focal length	50 mm
Half Field of view	$7.012^\circ$
Pupil Diameter	9.091 mm

the center of the image and it highly degrades the infrared image quality. These two effects in infrared lenses generally analysed at the far end of the optical design after all of the optical powers, materials and positions are already determined without taking into account these effects. Hence, the design could have poor performance from both athermalization and narcissus perspective although it has a very good aberration performance. As a result, time consuming iterations and optimizations are needed in order to get a satisfactory performance. As an example, an infrared lens with the specifications given in Table 1.1 is assumed to be designed. Cold stop height is defined as the air thickness between detector array and detector cold stop in these specifications.

Two very simple optical designs satisfying the aforementioned optical specifications

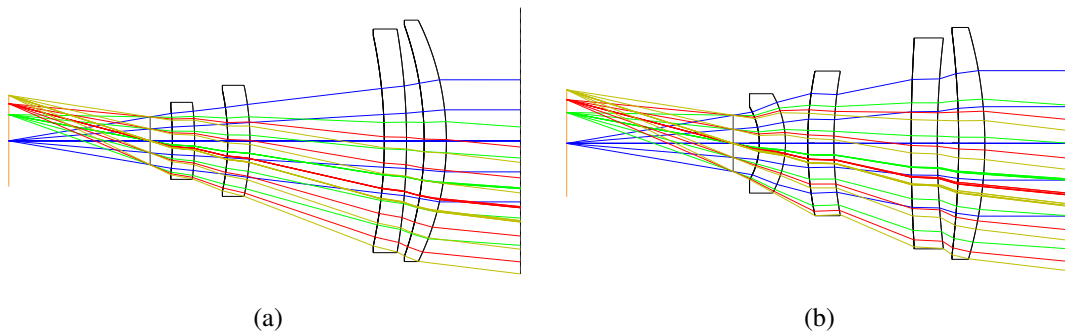


Figure 1.4: MWIR designs: (a) Design A, (b) Design B.

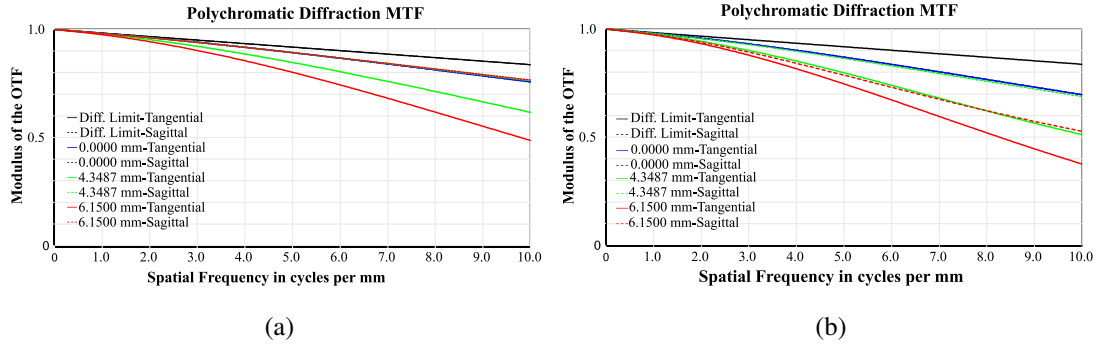


Figure 1.5: MTF performance of MWIR designs: (a) Design A, (b) Design B.

are shown in Fig. 1.4. Design A and B both consist of four lenses whose materials are germanium. In this thesis, Modulation Transfer Function (MTF) and spot size distributions are used in order to check the optical imaging quality of optical lenses. MTF is the contrast transferring ability of a lens from an object with a determined resolution to image. In other words, MTF is the frequency response of an optical system which acts similar to a low pass filter. MTF performances of these two designs are given in Fig. 1.5. These two designs have very similar MTF performance and look very similar to each other. However when the narcissus performances of these designs are analysed, it is found that there is a dramatic difference. Narcissus performances of these designs are given in Fig. 1.6. Narcissus performance is analysed in terms of temperature difference and abbreviated as Narcissus Induced Temperature Difference (NITD). This narcissus performance criterion will be used throughout this thesis. Narcissus is measured in terms of scene temperature difference. Since infrared optical system sensitivity is measured in terms of temperature difference, comparing narcissus performance with infrared system sensitivity is relatively easy. Narcissus performance of an infrared lens is given in NITD graphs, in which horizontal axis represents the detector position in radially outward direction starting from the center of the detector while vertical axis represents the NITD value in Kelvins.

As can be deduced from the narcissus performances of design A and B, while design A has a nearly 0.884 K narcissus performance which is totally unacceptable, design B has a nearly 0.017 K narcissus performance which is nearly perfect. Even in such a relatively simple optical configuration, it is highly possible to come up with such an

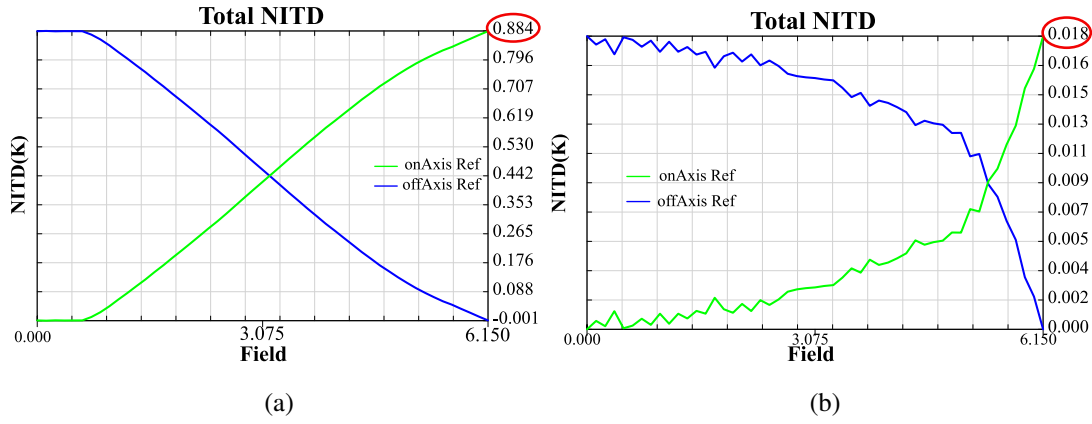


Figure 1.6: Narcissus performance of MWIR designs: (a) Design A, (b) Design B.

unacceptable narcissus performance. Although, it is a relatively easy task to switch from design A to design B at the optimization stage without the need to take narcissus considerations in the layout and thin lens stage, it is a very time consuming work to find a solution with a satisfactory narcissus performance at the optimization stage for highly complex optical designs.

As a result, although optical designs can perform a very satisfactory performance from aberration perspective and even look very close to each other, their narcissus performances do not have to be similar to each other. As in the aforementioned example, while one of them has a superior narcissus performance, the other can have a narcissus performance which makes the optical system totally unusable because of the highly disturbing narcissus effect in the infrared image. Hence, it is very important to consider narcissus effect in the early design stages of the optical lens so that time consuming iterations and optimizations are avoided. The main motivation of this thesis is to construct a mathematical model of narcissus effect which enables optical designers to include narcissus performance of a lens in the layout and thin lens design stages of the optical lens.

## 1.2 Proposed Methods and Models

At the layout and thin lens design stage, paraxial lenses which have no aberration are used in order to represent the optical design. These paraxial lenses operate ideally



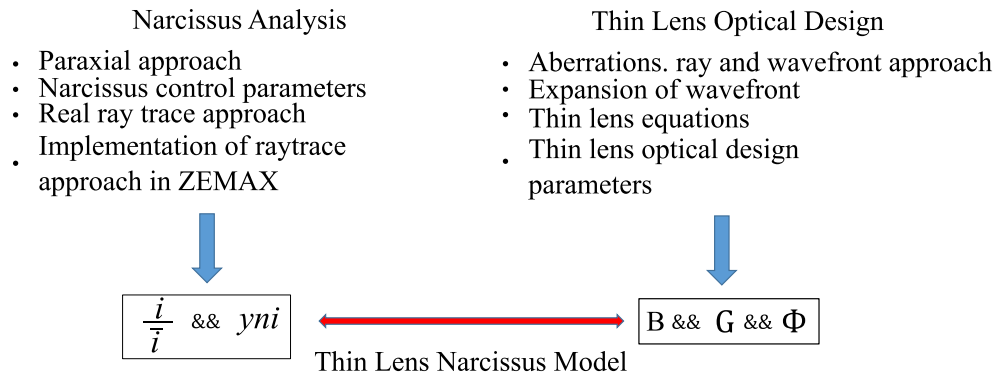


Figure 1.7: Thin lens narcissus model.

in a certain object image conjugates, hence satisfy optical specifications. In order to transform these paraxial lenses into real lenses with a definite geometrical shape and optical material, Seidel aberrations are used. Seidel aberration coefficients represent the third order optical aberrations in an optical design. These are the coefficients of the third order terms in the polynomial expansion of the wavefront error of an optical lens. Seidel coefficients are expressed in terms of the optical parameters of paraxial lenses which form the optical design. These optical parameters are conjugate factor, shape factor, optical power, material index and material Abbe number. Narcissus performance is controlled by two optical parameters for each optical lens surface in an optical design. Magnitude of the narcissus distribution is related with marginal ray angle of incidence at a surface while variation of the narcissus distribution is related with both marginal ray angle of incidence and chief ray angle of incidence at a surface. On one hand, there are Seidel aberration coefficients which are very useful for aberration control in layout and thin lens design stage. On the other hand, there are narcissus control parameters which are very useful at the optimization stage. These two aspects of infrared lens design are shown in Fig. 1.7.

In order to control narcissus performance at the early design stages of optical lens, a mathematical model which proposes two narcissus metrics in terms of optical parameters of paraxial lenses is constructed using mainly paraxial optics in this thesis. Although the proposed thin lens narcissus model controls the narcissus performance in the early design stage, it does not calculate the exact final narcissus distribution of an infrared lens. In order to calculate the final narcissus performance of an infrared

lens, a macro which is previously coded in ZEMAX Programming Language (ZPL) is used widely [10, 11].

### 1.3 The Outline of the Thesis

Narcissus phenomenon in infrared lens utilizing cooled infrared detectors is discussed in detail in Chapter 2. Different examples of infrared images with severe narcissus effect are given and general root causes of narcissus effect are studied with mathematical relations in detail. Conventional narcissus control techniques and parameters are introduced and examples related to these control techniques are given.

Thin lens aberration theory is briefly discussed based on Seidel coefficients in Chapter 3. Similar to Seidel coefficients, two narcissus metrics which form the proposed narcissus model are derived in terms of paraxial optical quantities of the paraxial lenses which are shape factor, conjugate factor, optical power, chief and marginal ray height in infrared optical system.

A fictitious infrared lens operating in Longwave Infrared (LWIR) band is designed systematically in Chapter 4 as an example to the proposed narcissus model. First, optical specifications namely focal length, field of view,  $f_{\#}$ , operating wavelength and detector details are defined. According to the defined optical specifications, a suitable optical architecture is chosen and paraxial form of the optical system is constructed. Lens number, optical powers and materials are determined such that focal length is satisfied and shape independent aberrations namely field curvature, axial and lateral colour aberrations are corrected sufficiently. Second, lens shape factors are optimized in order to correct shape dependent aberrations which are spherical aberration, coma, astigmatism and distortion. After shape factors of paraxial lenses are optimized, paraxial lenses are transformed to real lenses by introducing curvatures to them. At this point, image quality is checked with the help of ZEMAX spot size and MTF routines, while narcissus performance is checked with the abovementioned narcissus macro. Finally, center thicknesses are introduced to the real lenses with no thickness by utilizing a few cycles of optimization in order for them to carry optical power. MTF, spot size and narcissus performance are checked again and it is

shown that LWIR lens has near diffraction limited performance from imaging quality perspective and narcissus distribution at the detector plane of LWIR lens is below the sensitivity of the LWIR detector. This thesis study is concluded in Chapter 5.



## CHAPTER 2

### NARCISSUS EFFECT AND ITS ANALYSIS TECHNIQUES

Narcissus effect which is one of the most important differences between visible lenses and infrared lenses and its main causes are discussed in detail in Section 2.1. Afterwards, narcissus analysis techniques of an infrared lens utilizing cooled infrared detectors are mentioned in Section 2.2.

#### 2.1 Narcissus Effect and Its Causes

Narcissus effect is first discussed by Llyod in 1975 [12]. Llyod called narcissus effect as cold reflections. This effect shows itself as a dark disk-like shape in infrared images. Two examples of infrared images with severe narcissus effect are given in Fig. 2.1 [4, 5].

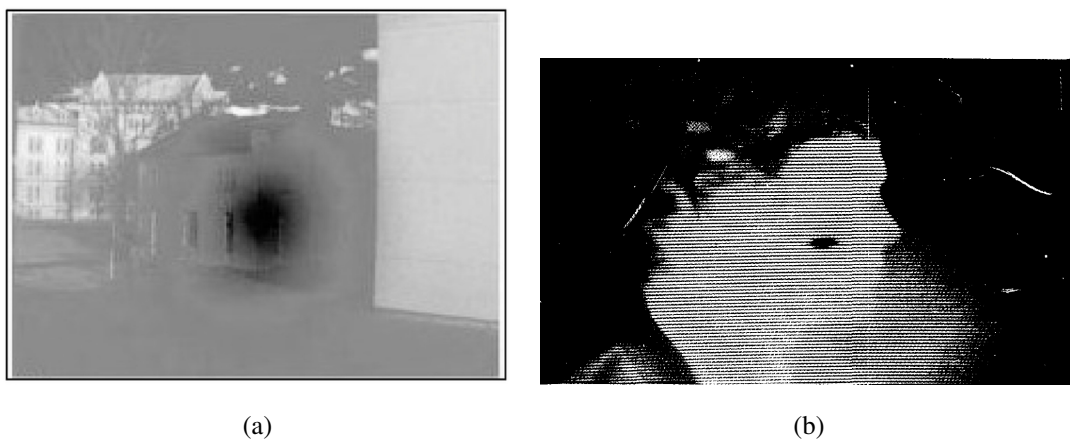


Figure 2.1: Infrared images with severe narcissus effects [4, 5].

Table 2.1: Infrared transmitting materials [1].

		$n_{4\mu m}$	$n_{10\mu m}$
Germanium	Ge	4,0245	4,0032
Silicon	Si	3,4255	-
Zinc selenide	ZnSe	2,4331	2,4065
Zinc Sulfide	ZnS	2,2518	2,2001

If narcissus is not controlled and analysed in infrared optical lens with cooled detectors, it highly degrades the quality of infrared images such that infrared imaging system cannot be used. Infrared imagery is based on the thermal self-emission of objects to be imaged. Hence, performance of an infrared imaging system is quantified as the minimum temperature difference which can be resolved. In order to increase the sensitivity of infrared systems, different types of noises must be reduced. One of the main noise is the generation-recombination noise which is the statistical fluctuation in the rate of generation and recombination of charged particles within the detector [13]. In order to reduce these types of noises in infrared detectors, detectors are cooled to cryogenic temperature levels. Although noise levels are reduced satisfactorily, a considerable temperature difference is now introduced between detector and opto-mechanical housing of the infrared lens. Because of this temperature difference, cold detector acts similar to sun in visible imaging systems which causes unwanted significant contrast differences in images. As a result, narcissus image is formed by the retro-reflections of the cold detector from refractive lenses back onto itself. The temperature difference between detector and opto-mechanical housing is the first main reason of the narcissus effect in infrared imagery.

Visible glasses cannot be used in infrared lenses since majority of them absorb infrared radiation. Hence, different types of infrared transmitting materials are used instead of visible glasses in infrared lenses. Although there are a wide range of materials which transmit infrared radiation, some of them have excellent properties. Most widely used infrared lens materials are silicon, germanium, zinc sulfide and zinc selenide. Refractive indices and Abbe numbers of these materials are given in Table 2.1 [1]. Refractive indices of infrared transmitting materials are much greater than

visible glass materials. Due to the Fresnel reflection losses in materials, there is a significant Fresnel loss in infrared lenses because of the higher refractive indices with respect to visible lenses. Hence, anti-reflection coatings are much more important in infrared lenses and must be applied to each and every refractive surfaces in infrared lens systems. Although very efficient anti-reflective coatings are designed and applied to the refractive surfaces, there is still residual reflections in these coatings which enable considerable amount of retro-reflections of cold detector to reach cold detector itself and create an unwanted contrast difference in infrared image. Residual reflection of anti-reflective coatings applied to infrared lenses is the second cause of narcissus effect in infrared lenses with cooled detectors.

Since narcissus effect is a result of retro-reflections of cold detector from refractive surfaces, narcissus distribution on the detector is directly related with the bending of the lenses. Narcissus spot distributions of a surface in a typical infrared lens with two different bendings are given in Fig. 2.2. As shown in the figure, depending on the curvature of the retro-reflecting surface, narcissus distribution changes drastically. This is the main reason of very different narcissus performing infrared lenses could perform similarly from aberration perspective. Lens bending is the last reason of the narcissus effect in infrared lenses.

There are a few High Operating Temperature (HOT) detectors in the market [14]. However, their detector operating temperature is around 150 K which is still very far away from the room temperature. Hence, narcissus effect must still be analyzed and controlled even in these type of HOT detectors. In a similar way, although very low back reflection coatings are developed in infrared spectrum, narcissus can still be very dominant and disturbing in infrared images. It is not possible to totally eliminate back reflections from refracting surfaces of infrared lenses, as a result narcissus reduction is still mandatory in infrared lenses. As in the aberration correction of lenses, lens bending is the most effective tool in narcissus reduction in infrared lens design.

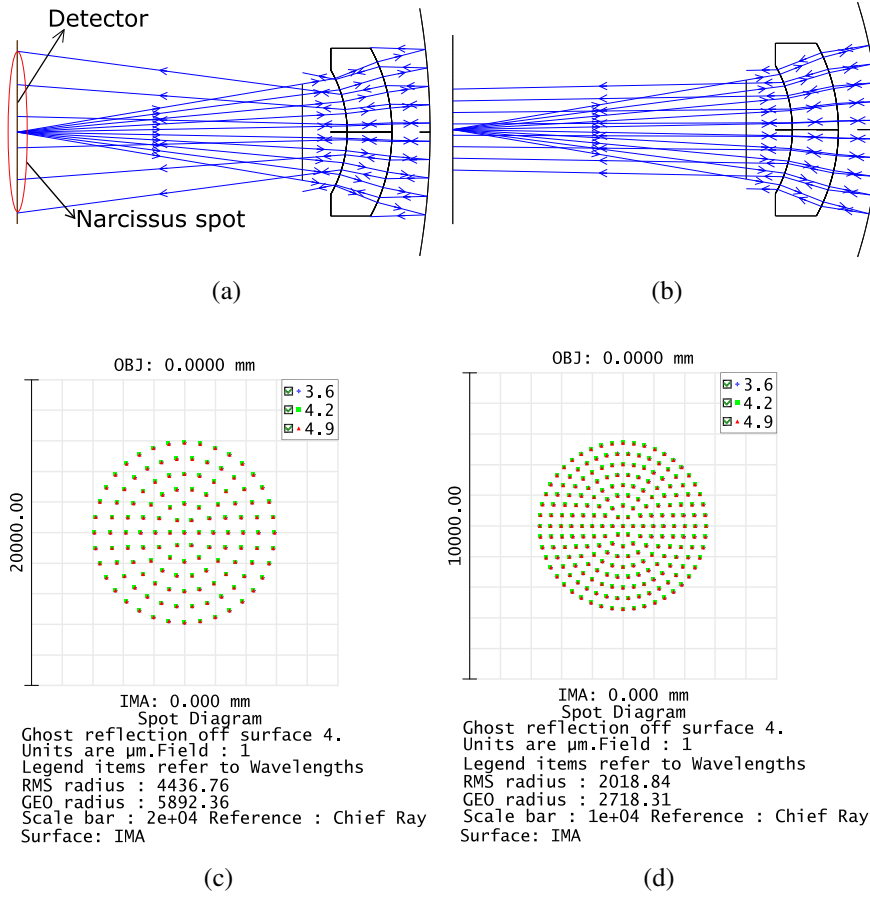


Figure 2.2: Narcissus spots with two different surface curvatures.

## 2.2 Narcissus Analysis and Control Techniques

As stated previously, narcissus effect stems from the retro-reflections of cold detector onto itself from refractive surfaces in an infrared system. Hence, spot size of these ghost returns and variation of these ghost returns with respect to field of view are strongly correlated with the narcissus performance of an infrared lens. Howard and Abel derived paraxial surface-contribution formulas for the aforementioned spot size and variations of narcissus ghosts [5]. They constructed a Lagrange invariant with forward traced marginal ray and reflected marginal ray at a narcissus contributing surface. As a result, they showed that narcissus spot radius at the detector is given by:

$$y_{r'} = -4ynif_{\#} \quad (2.1)$$



Table 2.2:  $y_{ni}$  based and real-ray trace based ghost spot radius.

Surface	$y_{ni}$	Paraxial ghost spot radius	Real-ray trace ghost spot
2	0.149	1.792	1.759
3	-0.063	-0.767	0.770
4	-0.122	-1.472	1.475
5	0.673	8.077	7.891
6	0.264	3.169	3.136
7	-2.202	-26.424	36.000

where  $y$  is the marginal ray height,  $n$  is the refractive index of the medium,  $i$  is the marginal ray angle of incidence and  $f_{\#}$  is the speed of the lens. A typical 3 lens MWIR system with an  $f_{\#}$  value 3 is shown in Fig. 2.3. Paraxial  $y_{ni}$  values, paraxial ghost spot radius and real-ray trace based ghost spot radius are given in Table 2.2. Eq. 2.1 is an effective way of calculating the narcissus spot radius in an infrared lens. Since  $f_{\#}$  is fixed in a given infrared lens, paraxial  $y_{ni}$  values of lens surfaces are very important in controlling the magnitude of narcissus effect. As  $y_{ni}$  value of a surface increases, narcissus spot size stemming from contributing surface also increases which implies that the ghost image of the cold detector is defocused more. As a result, in order to reduce the narcissus contribution of a surface, its  $y_{ni}$  value must be increased. Second parameter of narcissus to be controlled is the variation of the narcissus distribution at the detector. Variation of narcissus effect is strongly

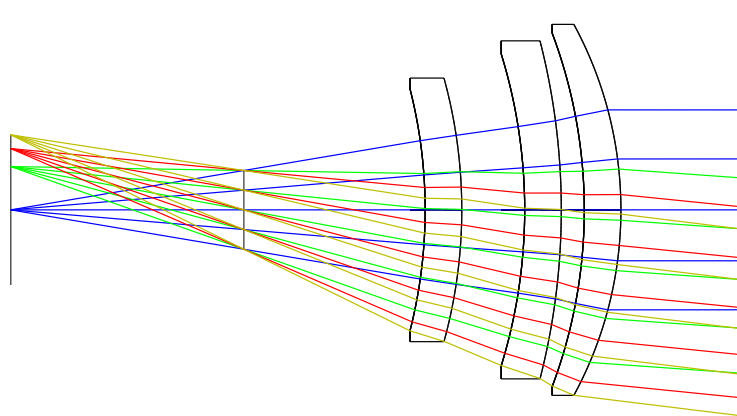


Figure 2.3: A typical 3 element MWIR lens.

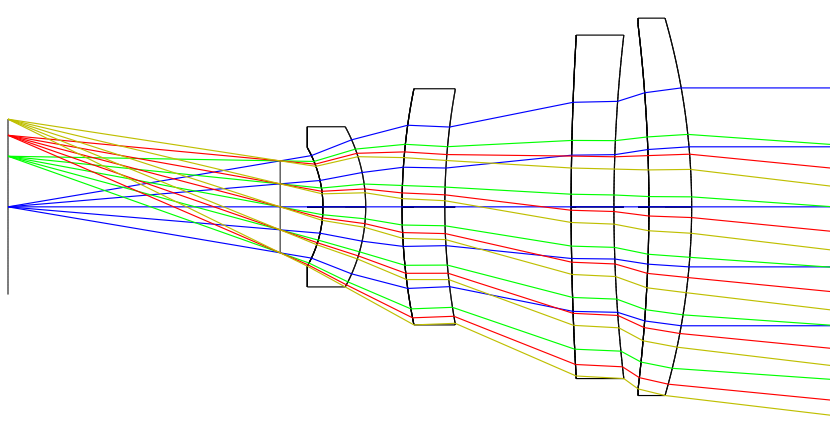


Figure 2.4: A typical 4 element MWIR lens.

related with the deviation of narcissus ghost spot within the field of view. Howard and Abel proposed a paraxial formula for the variation of narcissus by utilizing two different Lagrange invariant in an infrared lens [5]. They constructed first invariant by using forward marginal ray and the reflected backward-traced chief ray, second invariant by using forward marginal ray and chief ray. As a result, they calculated the chief ray height ( $\bar{y}_r'$ ) as follows:

$$\bar{y}_r' = -4yn\bar{i}f_{\#} \quad (2.2)$$

where  $\bar{i}$  is the chief ray angle of incidence. Finally, variation of the narcissus distribution is related with the ratio of reflected marginal ray height at the detector ( $y_r'$ ) and reflected chief ray height at the detector ( $\bar{y}_r'$ ) which gives the second paraxial narcissus control parameter  $i/\bar{i}$ . Optimizing this second parameter to be greater than 1 is generally sufficient for controlling the variation of narcissus distribution across the detector.

A typical MWIR system with 4 lens is shown in Fig. 2.4. In this lens, curvature of the first surface of second lens is intentionally changed in order to investigate the effect of second control parameter  $i/\bar{i}$ . Since narcissus variation across the detector is inter-related with the vignetting, vignetting plots are analyzed and given in Fig. 2.5 with respect to different  $i/\bar{i}$  values by changing the curvature of the narcissus contributing surface. As can be deduced from the figure, variation of the narcissus distribution decreases as  $i/\bar{i}$  value of narcissus contributing surface increases. Vignetting is the

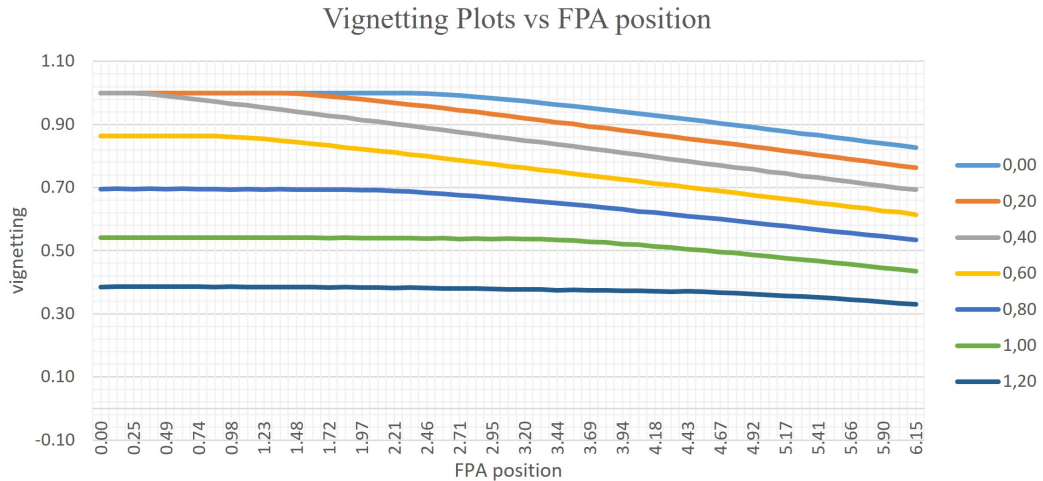


Figure 2.5: A typical vignetting plot for different  $i/\bar{i}$  values.

clipping of rays in an optical lens because of the insufficient geometrical dimensions of opto-mechanical housing and lenses. Because of the fact that vignetted rays see the hot opto-mechanical housing while the rest see cold detector dewar structure, vignetting plot is closely related to the narcissus distribution in an infrared lens with cooled detector. Focal Plane Array (FPA) geometry is generally in rectangular form and optical lenses are mostly designed in rotationally symmetric manner which enables optical lenses to have capability to illuminate a circular region at the FPA position. Rotational symmetry of the optical lenses is used in optical design in order to increase the efficiency of the ray trace. Hence, the field of view assigned in optimization and analysis is assigned radially outward in diagonal direction of the FPA. As a result, all the optical and narcissus performance of the infrared lens are calculated with respect to the diagonal position at the FPA in this thesis.

The abovementioned paraxial parameters are very beneficial in controlling narcissus from optical design perspective. There are also other methods which are proposed previously. Howard and Abel proposed using optical filter which discriminates the scene spectrum from narcissus spectrum in order to block narcissus radiation while the spectrum of the scene is undisturbed [5]. In majority of today's infrared military systems, optical system is already filtered by efficient band-pass cold filters at the detector level such that only interested spectrum is allowed to transmit. Lloyd and Lau proposed to compensate the cold detector by using a hot object with a beamsplitter in

the optical path [12, 15]. Hence, all the cold portion of the detector is compensated by the hot object and the narcissus effect is eliminated. However, by putting a beam-splitter at the optical path, scene radiation is also reduced. As a result, total system performance is unacceptably degraded. Lloyd also proposed a warm baffling in order to reduce the radiating part of the detector [12]. This technique is especially very effective in relayed infrared systems by putting an narcissus field stop at the internal image plane.

Although paraxial control parameters discussed previously are very effective in controlling narcissus, it is not possible to construct the final narcissus distribution or narcissus image, which will be seen when the optical lens under design is built, by just using these paraxial narcissus control parameters even though narcissus is controlled to a satisfactory level. Hence, it is very important to construct an analysis method in order to get an image of narcissus distribution at detector level in terms of the scene temperature difference after optical design is finished. Narcissus is expressed verbally as follows [16]:

$$NITD = \frac{\left( \begin{array}{c} \text{projected} \\ \text{solid angle} \\ \text{of narcissus} \\ \text{return} \end{array} \right) \times \left( \begin{array}{c} \text{reflectivity} \\ \text{of narcissus} \\ \text{surface} \end{array} \right) \times \left( \begin{array}{c} \text{transmission} \\ \text{from detector to} \\ \text{narcissus surface} \end{array} \right)^2 \times \left( \begin{array}{c} \text{inband} \\ \text{blackbody} \\ \text{emission at} \\ \text{background} \\ \text{temperature} \end{array} \right)}{\left( \begin{array}{c} \text{projected solid} \\ \text{angle of scene} \\ \text{energy} \end{array} \right) \times \left( \begin{array}{c} \text{optics} \\ \text{transmission} \end{array} \right) \times \left( \begin{array}{c} \text{inband} \\ \text{blackbody} \\ \text{emission change} \\ \text{for scene } \Delta T \end{array} \right)} \quad (2.3)$$

A mathematical equation which gives NARC- $\Delta T$  which is the narcissus in terms of scene temperature difference of a scanning infrared lens system is proposed by Howard and Abel [5]. They expressed narcissus as:

$$NARC-\Delta T = \sum_{\text{all lens surfaces}} \frac{C_j \int_0^\infty L(\lambda, T_h) \tau_j^2(\lambda) R_j(\lambda) \xi(\lambda) d\lambda}{\int_0^\infty \frac{\partial L(\lambda, T_s)}{\partial T} A(\lambda) \tau_s(\lambda) \xi(\lambda) d\lambda} \quad (2.4)$$

where  $j$  is the surface number,  $C_j$  is the cold return from the surface  $j$ ,  $\tau_j$  is the transmittance of the optics from the detector to the surface  $j$ ,  $R_j$  is the reflectance of surface  $j$ ,  $T_h$  is the housing temperature,  $T_s$  is the scene temperature,  $\tau_s$  is the transmittance of the optical system,  $\xi$  is the responsivity of the detector,  $L$  is the Planck's blackbody radiance. Cold return abbreviated as  $C_j$  is given by:

$$C_j = \frac{\epsilon M}{\pi(4ynif\#)^2} \quad (2.5)$$

For staring infrared system, similar approach to Eq. 2.4 is proposed by Akram as follows [17]:

$$NITD_{ij} = \frac{\int_{\lambda_1}^{\lambda_2} [N(\lambda, T_H) - N(\lambda, T_D)] R_d(\lambda) d\lambda t_j^2}{\int_{\lambda_1}^{\lambda_2} \frac{\partial N(\lambda, T_{MS})}{\partial T} R_d(\lambda) d\lambda} \frac{t_j^2}{t_o} R_j \sigma_{ij} \quad (2.6)$$

where  $\lambda_1$  and  $\lambda_2$  are operating wavelengths,  $T_H$  is the housing temperature,  $T_D$  is the detector temperature,  $N(\lambda, T)$  is Planck's spectral blackbody radiance,  $T_{MS}$  is the mean scene temperature,  $R_d(\lambda)$  is the normalized detector spectral responsivity,  $t_j$  is the average optics transmission starting from the detector surface up to the narcissus contributing lens surface,  $t_o$  is the optical transmission,  $R_j$  is the surface reflectivity of the surface under consideration,  $\sigma_{ij}$  is the surface cold return.  $\sigma_{ij}$  is the ratio of the solid angle of the cold radiation returned to the detector after reflecting from the surface under consideration to the solid angle of the cold stop of the detector which is the energy gathering capacity of the infrared lens.  $\sigma_{ij}$  is calculated by tracing rays starting from the  $i$ 'th pixel position of the detector, reflecting from the  $j$ 'th surface under consideration and finally up to the detector back itself in the narcissus single bounce ghost file of the  $j$ 'th surface under consideration. Then, vignetting value is equal to the cold return ratio.

In ZPL platform, a narcissus calculating macro is coded which uses Eq. 2.6 [10]. In order to calculate narcissus distribution at the detector, narcissus single bounce ghost files must be created beforehand. Then, housing temperature, scene temperature and detector temperature must be entered by user. Each single bounce narcissus ghost file is called and vignetting plots are calculated. Finally, 1D and 2D narcissus distribution at the detector level and surface contributions are plotted. Typical outputs of the macro are given in Fig. 2.6. Details of the code are given in Appendix A.

Narcissus macro implemented in ZEMAX platform assumes rotational symmetry in the optical design which imposes a strong restriction to the narcissus analysis of infrared optical systems with cooled detectors. Although majority of the infrared optical designs are rotationally symmetric, there are many examples of infrared optical designs with bilateral symmetry or even with no symmetry. Hence, an alternative method of analyzing the final narcissus image in infrared systems with cooled detectors is implemented in FRED scripting platform by applying clever tricks proposed by Pfisterer [18]. Narcissus effect is actually the thermal emission of optics itself.

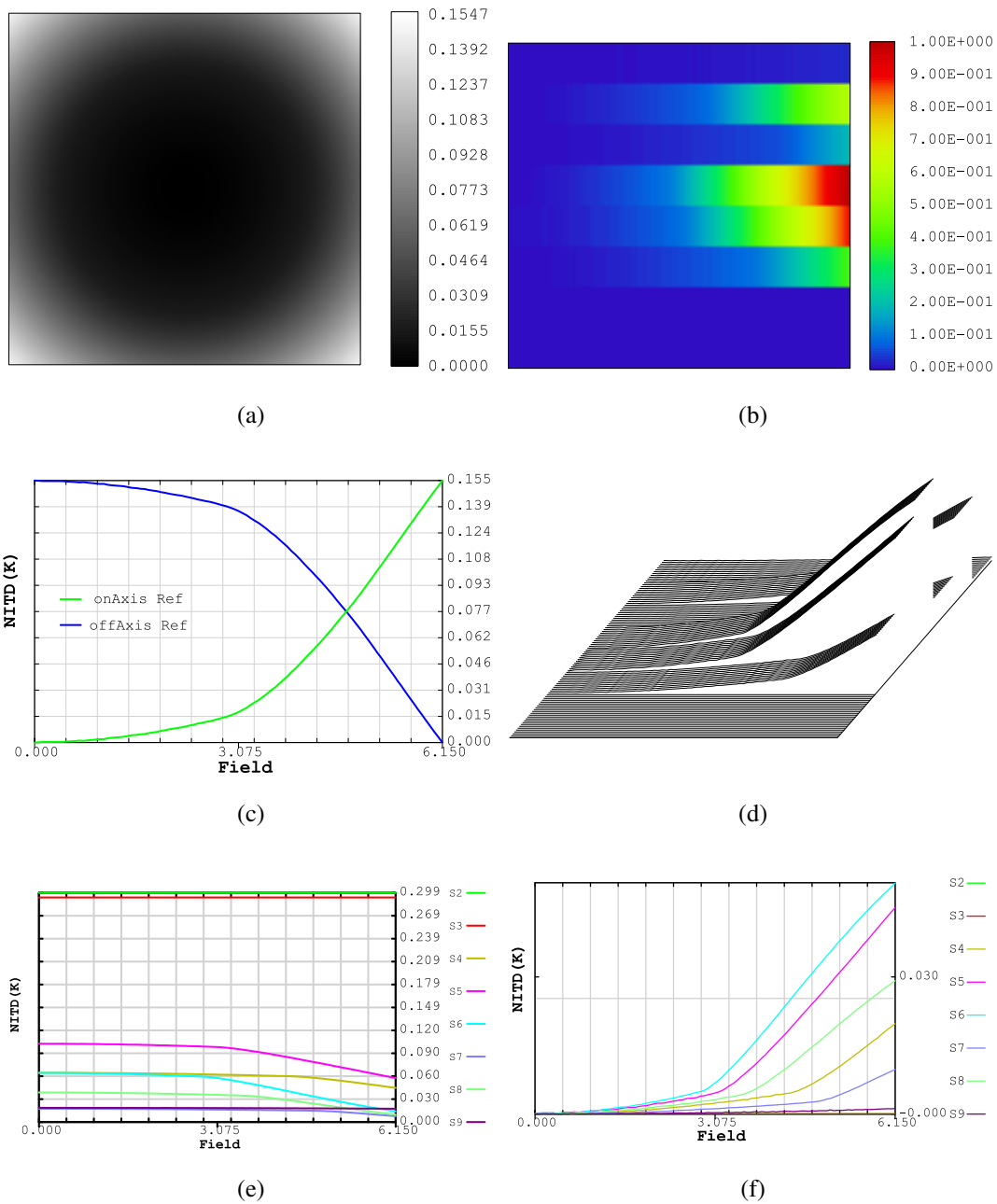


Figure 2.6: Narcissus macro outputs: (a) Narcissus distribution at the FPA (2D plot), (b) Surface narcissus contributions (false color plot), (c) Narcissus curve through half diagonal of the detector, (d) Surface narcissus contributions (3D plot), (e) Surface narcissus contribution curves through half diagonal of the detector (without correction), (f) Surface narcissus contribution curves through half diagonal of the detector (with correction).

Therefore, narcissus analysis is also defined as Thermal Self-Emission (TSE) analysis. Thermal self-emission of an object in an optical design is expressed as follows:

$$TSE = \sum_{\text{all objects}} L_{\text{object}} A_{\text{object}} \Omega_{\text{detector}} \quad (2.7)$$

where  $L_{\text{object}}$  is the radiance of the emitting object,  $A_{\text{object}}$  is the area of the emitting object and  $\Omega_{\text{detector}}$  is the solid angle of the detector seen by the object.  $L_{\text{obj}}$  can be easily written as follows:

$$L_{\text{object}} = \frac{\epsilon f \sigma T^4}{\pi} \quad (2.8)$$

where  $\epsilon$  is the emissivity of the emitting object,  $\sigma$  is Stephan-Boltzmann constant,  $T$  is the temperature of the emitting object and  $f$  is the fractional blackbody which is given as

$$f = \frac{\int_{\lambda_1}^{\lambda_2} L_{BB}(T, \lambda) d\lambda}{\int_0^{\infty} L_{BB}(T, \lambda) d\lambda} \quad (2.9)$$

where  $L_{BB}$  is the radiance of blackbody given by Planck's blackbody radiation equation. Main difficulty is the calculation of  $A_{\text{object}}$  and  $\Omega_{\text{detector}}$ . Although it is possible to assign Lambertian emitter and emissivity to objects in optical design and trace rays in order to calculate power reaching the infrared detector in FRED, it requires a large number of rays to be traced in order to get sufficient results because of the small solid angle of the detector seen by the emitting object. In order to increase the efficiency of the TSE analysis, reciprocity is applied. Using the reciprocity rule in Eq. 2.7, TSE is expressed as follows:

$$TSE = \sum_{\text{all objects}} L_{\text{detector}} A_{\text{detector}} \Omega_{\text{object}} \quad (2.10)$$

Since radiance is conserved in an optical system, TSE can be written as:

$$\begin{aligned} TSE &= \sum_{\text{all objects}} L_{\text{object}} A_{\text{detector}} \Omega_{\text{object}} \\ &= \sum_{\text{all objects}} \frac{\epsilon f \sigma T^4}{\pi} A_{\text{detector}} \Omega_{\text{object}} \\ &= \sum_{\text{all objects}} \epsilon f \sigma T^4 A_{\text{detector}} \frac{\Omega_{\text{object}}}{\pi} \end{aligned} \quad (2.11)$$

All of the parameters in Eq. 2.11 are known except  $\Omega_{\text{object}}$  which is the solid angle of the emitting object seen by the detector. In order to calculate the solid angle of the emitting objects efficiently, radiance equation is written as follows:

$$P_{\text{object}} = L_{\text{detector}} A_{\text{detector}} \Omega_{\text{object}} \quad (2.12)$$

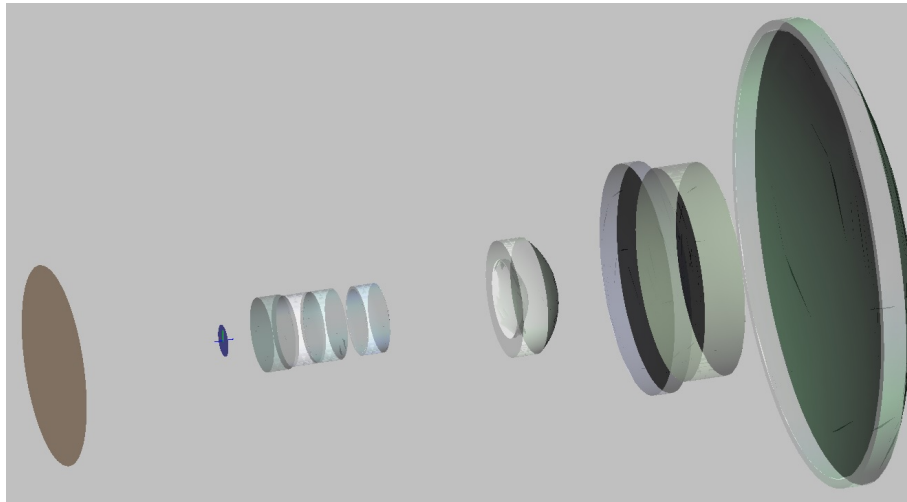
If a source with radiance  $L = \frac{1}{\pi A_{\text{det}}}$  is created at the detector pixel position, then projected solid angle of the object seen by the detector ( $\frac{\Omega_{\text{object}}}{\pi}$ ) will be numerically equal to the power absorbed by the emitting object. Total power to be assigned to the source assuming radiation is into a cone with half angle  $\theta$  is calculated as follows:

$$\text{Source Power} = \sin^2 \theta \quad (2.13)$$

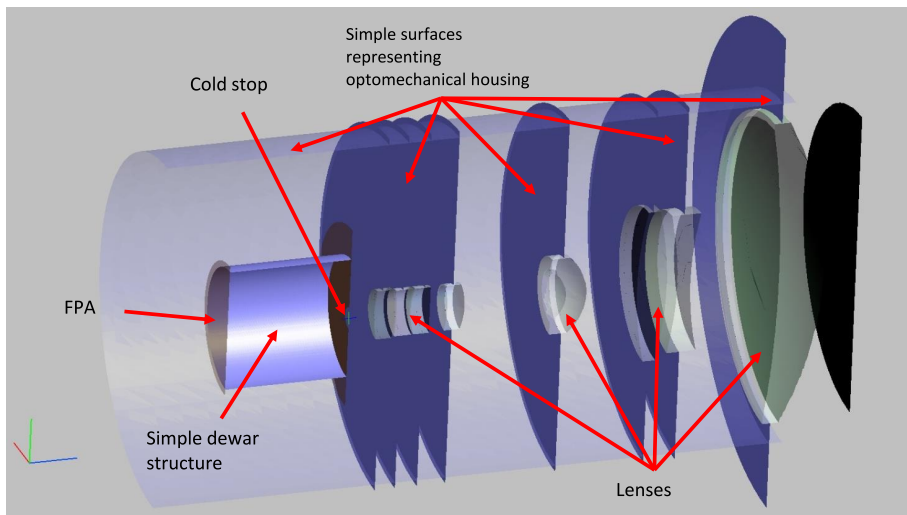
Once the projected solid angles of all emitting objects in an optical system are found, total narcissus image at the infrared detector can be easily analyzed. This analysis method is based on a radiometric method which benefits from the capabilities of FRED in calculating thermal self-emission of optical systems. An alternative method of analysing the final narcissus image in infrared systems with cooled detectors is also implemented in FRED scripting platform [19]. Details of the code is given in Appendix B. A typical setup for analysing narcissus effect in infrared lens systems with cooled detectors in FRED platform is given in Fig. 2.7. For the sake of simplicity, complex opto-mechanical and dewar structures are represented by simple geometrical surfaces.

Typical outputs of the script coded in Fred scripting environment are given in Fig. 2.8, 2.9, 2.10.



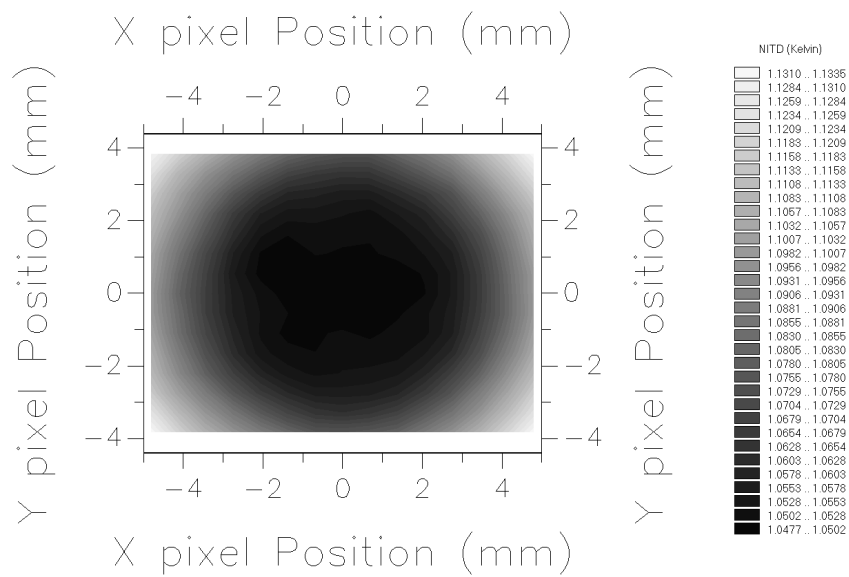


(a)

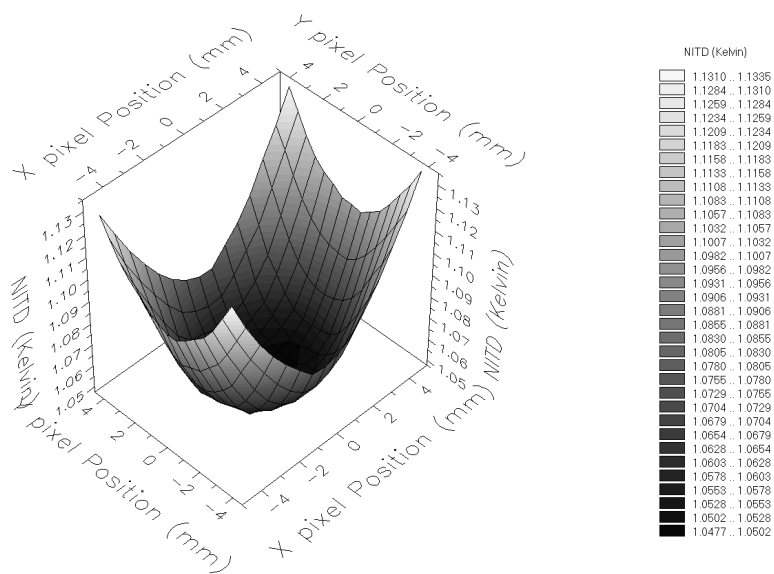


(b)

Figure 2.7: A typical simple infrared setup for narcissus analysis in FRED platform: (a) Optical design, (b) Optical design with opto-mechanical housing and detector dewar structure represented by simple geometrical surfaces.

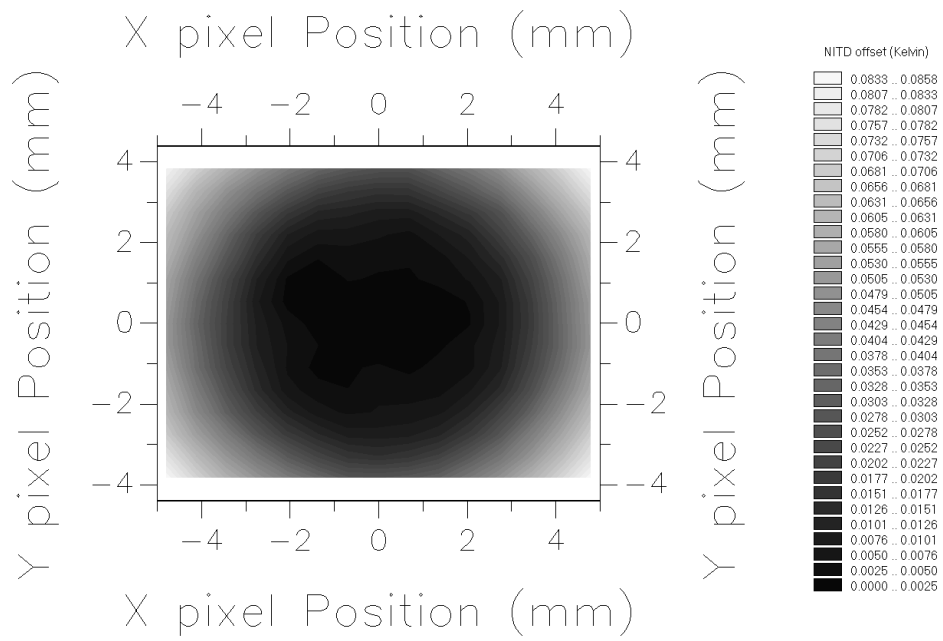


(a)

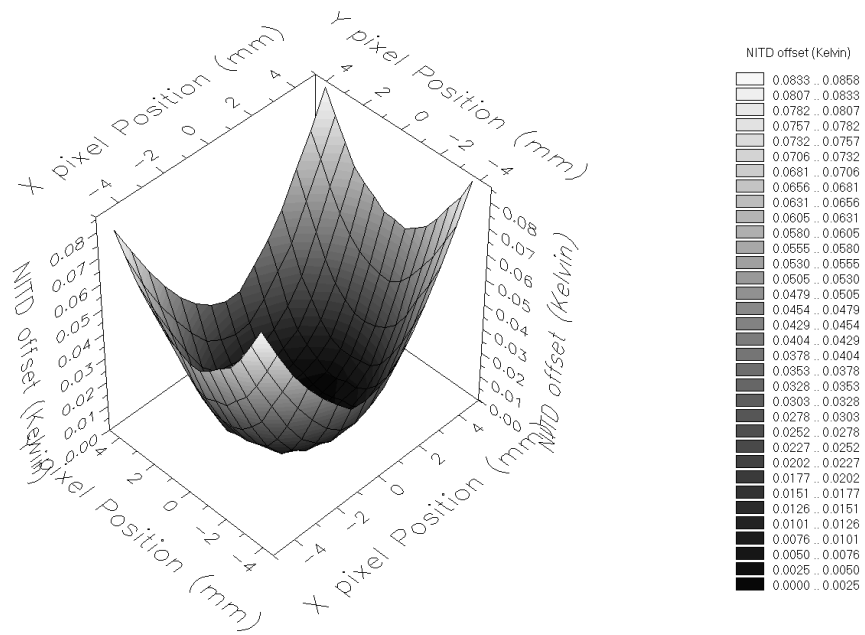


(b)

Figure 2.8: Outputs of narcissus analysing script coded in FRED scripting environment: (a) NITD distribution, (b) NITD (perspective view).



(a)



(b)

Figure 2.9: Offset corrected outputs of narcissus analysing script coded in FRED scripting environment: (a) NITD offset corrected distribution, (b) NITD offset corrected (perspective view).

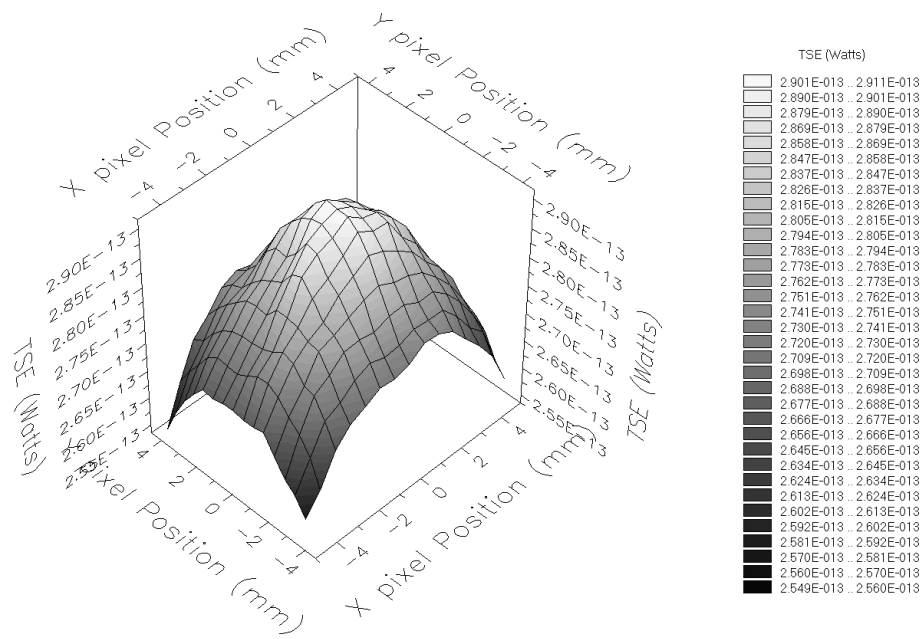
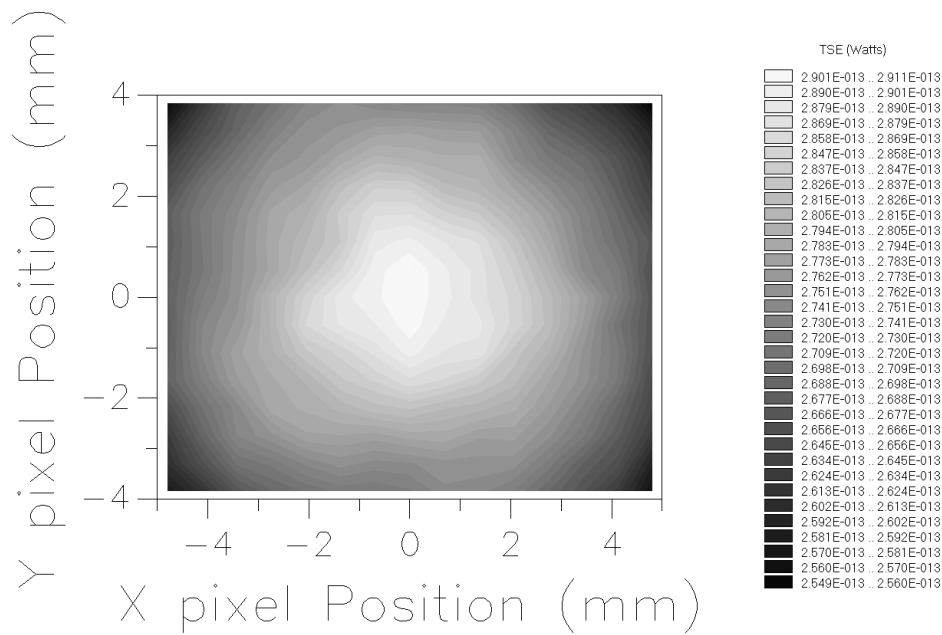


Figure 2.10: TSE outputs of narcissus analysing script coded in FRED scripting environment: (a) TSE distribution, (b) TSE (perspective view).

## CHAPTER 3

### THIN LENS NARCISSUS MODEL

#### 3.1 Seidel Aberration Theory

The main function of an optical system is to conjugate each and every point in object plane to another specific point in image plane at which a detector which is sensitive to the radiation emanating from the object is placed. Ideally, every point in object plane has a corresponding point in image plane. However, each point in object plane is imaged as a cloud of points instead of a perfect point in real optical systems because of the optical aberrations stemming from the structure of the optical elements forming the optical system. The main work of an optical lens designer is to correct these aberrations in an optical system in order to get an imaging quality which satisfies the optical specifications defined. A typical aberration of a real lens is shown in Fig. 3.1 with real ray tracing.

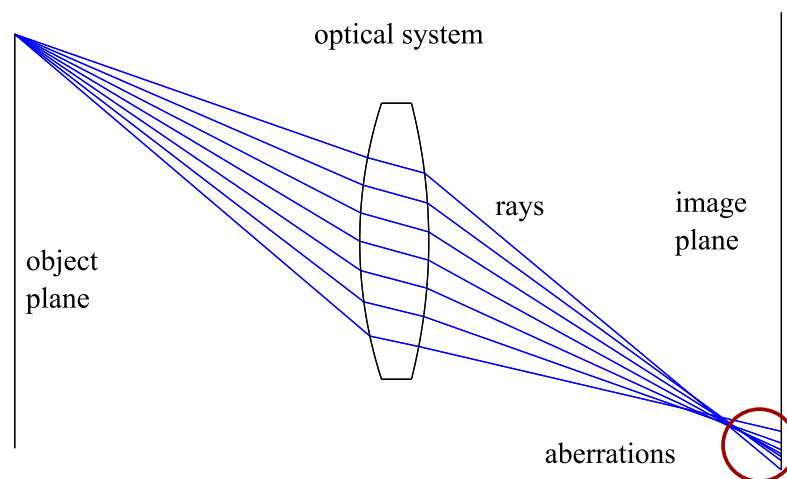


Figure 3.1: A typical optical aberration of a real lens.

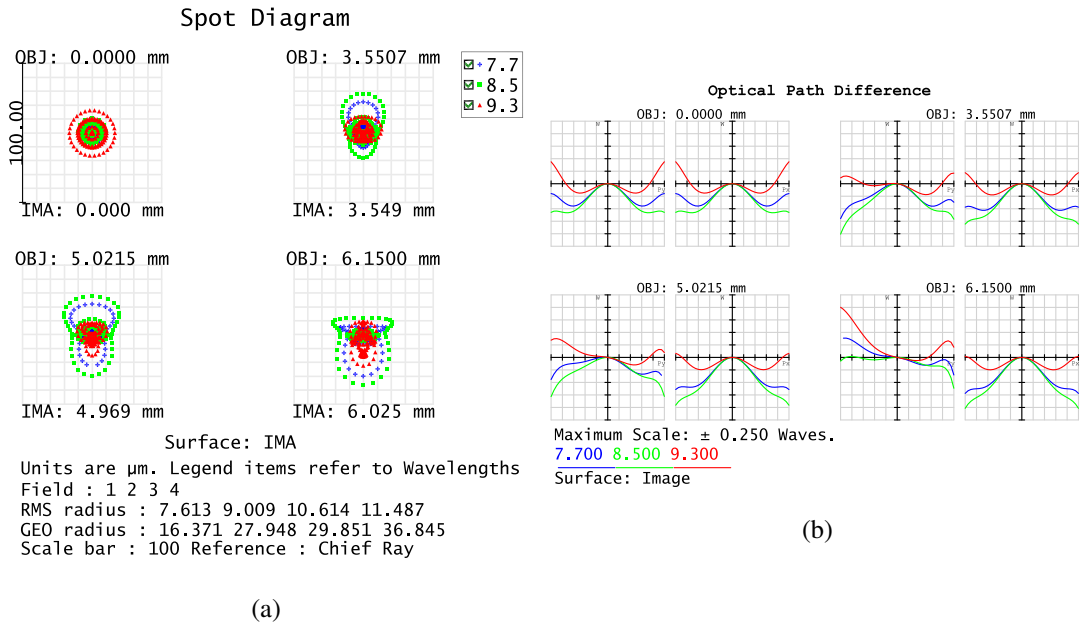


Figure 3.2: Aberration representations: (a) Spot diagram, (b) Optical Path Difference (OPD) fan.

Optical aberrations can be viewed in two different perspectives. First one is the physical positions of rays at image plane corresponding to a field point. Rays or pencils emanating from the object point are workhorses in this view. Each and every ray starting from the object point is traced up to the image plane and the positional deviations of all rays from the reference position is calculated and a point cloud is drawn. This point cloud is called the spot diagram of the corresponding field point. Spot diagrams are very useful in this aberration perspective. Although, this view of aberrations is perfect for visualizing, it is not suitable for differentiating the types of aberrations since most of the time all of the optical aberrations are intermixed. Second view is the deviation of the wavefront from the perfect sphere which is called the wavefront error. Points at the object field is represented by a perfect spherical wave centered at the position of the point. Rays emanating from the point source are perpendicular to this wavefront. Because of the aberrations of the real optical components, wavefronts transmitted or reflected from optical components deviate from perfect sphere. This deviation from perfect sphere is considered as wave aberration. OPD fans are very useful in this type of aberration consideration. A typical spot size distribution and OPD fan are shown in Fig. 3.2.

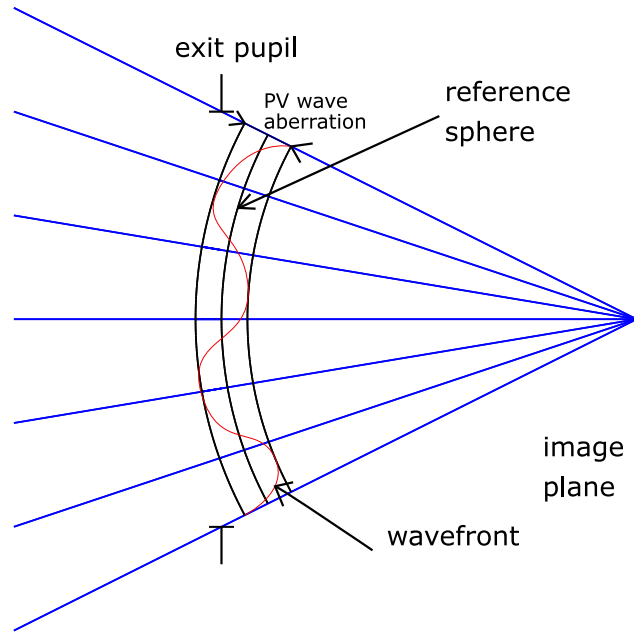


Figure 3.3: Wavefront aberration in an optical system.

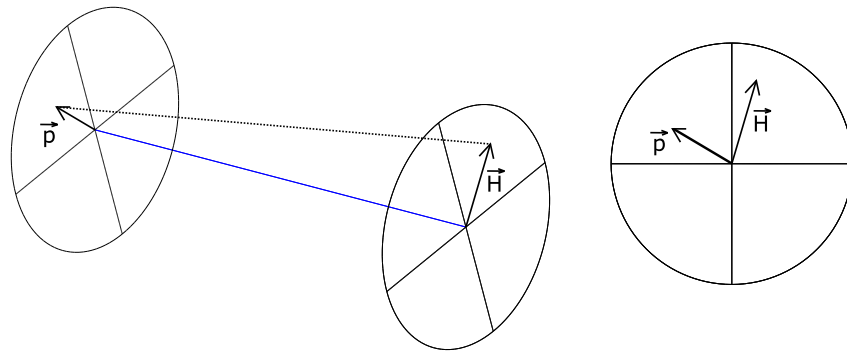


Figure 3.4: Field and pupil vectors in an optical system.

Wavefront representation of aberrations is mainly adopted in this thesis. Deviation of the wavefront from the perfect reference spherical wavefront at the exit pupil of the optical system is shown as an example in Fig. 3.3.

Wavefront error depends on the position of the object point in object space ( $\vec{H}$ ), position of ray in exit pupil ( $\vec{\rho}$ ) and the angle between these two vectors ( $\phi$ ) which are shown in Fig. 3.4.

Using rotational symmetry of optical systems, wavefront error can be written as  $W =$

$W(\vec{H} \cdot \vec{H}, \vec{H} \cdot \vec{\rho}, \vec{\rho} \cdot \vec{\rho})$ . Wavefront error of an optical system is expanded as a polynomial in terms of its dependent variables [20]. This expansion is given by R. Shack [21] as follows:

$$\begin{aligned}
W(\vec{H}, \vec{\rho}) &= \sum_{j,m,n} W_{k,l,m} (\vec{H} \cdot \vec{H})^j (\vec{H} \cdot \vec{\rho})^m (\vec{\rho} \cdot \vec{\rho})^n \\
&= W_{000} + W_{200}(\vec{H} \cdot \vec{H}) + W_{111}(\vec{H} \cdot \vec{\rho}) + W_{020}(\vec{\rho} \cdot \vec{\rho}) \\
&+ W_{040}(\vec{\rho} \cdot \vec{\rho})^2 + W_{131}(\vec{H} \cdot \vec{\rho})(\vec{\rho} \cdot \vec{\rho}) + W_{222}(\vec{H} \cdot \vec{\rho})^2 \\
&+ W_{220}(\vec{H} \cdot \vec{H})(\vec{\rho} \cdot \vec{\rho}) + W_{311}(\vec{H} \cdot \vec{H})(\vec{H} \cdot \vec{\rho}) + W_{400}(\vec{H} \cdot \vec{H})^2 \\
&+ W_{240}(\vec{H} \cdot \vec{H})(\vec{\rho} \cdot \vec{\rho})^2 + W_{331}(\vec{H} \cdot \vec{H})(\vec{H} \cdot \vec{\rho})(\vec{\rho} \cdot \vec{\rho}) \\
&+ W_{422}(\vec{H} \cdot \vec{H})(\vec{H} \cdot \vec{\rho})^2 \\
&+ W_{420}(\vec{H} \cdot \vec{H})^2(\vec{\rho} \cdot \vec{\rho}) + W_{511}(\vec{H} \cdot \vec{H})^2(\vec{H} \cdot \vec{\rho}) + W_{600}(\vec{H} \cdot \vec{H})^3 \\
&+ W_{060}(\vec{\rho} \cdot \vec{\rho})^3 + W_{151}(\vec{H} \cdot \vec{\rho})(\vec{\rho} \cdot \vec{\rho})^2 + W_{242}(\vec{H} \cdot \vec{\rho})^2(\vec{\rho} \cdot \vec{\rho}) \\
&+ W_{333}(\vec{H} \cdot \vec{\rho})^3
\end{aligned} \tag{3.1}$$

where  $k, l, m$  are integers and  $k = 2j + m, l = 2n + m$ . Aberration coefficients are represented by  $W_{klm}$ . Algebraic and vectorial notations of optical aberrations based on wavefront polynomial expansion are given in Table 3.1 [2].

Wavefront polynomial can also be expressed in terms of Seidel sums as follows:

$$\begin{aligned}
W(\rho, \phi, H) &= \frac{1}{8} S_I \rho^4 + \frac{1}{2} S_{II} H \rho^3 \cos \phi \\
&+ \frac{1}{2} S_{III} H^2 \rho^2 \cos^2 \phi \\
&+ \frac{1}{4} (S_{III} + S_{IV}) H^2 \rho^2 \\
&+ \frac{1}{2} S_V H^3 \rho \cos \phi
\end{aligned} \tag{3.2}$$

These Seidel sums are expressed in terms of ray trace parameters, refractive index of used materials and certain optical invariants. The main power of Seidel sums is that they can be used for paraxial lenses which are very useful for constructing initial starting points for designing optical systems. For paraxial lenses, Seidel sums when



stop is at the paraxial lens are expressed as follows:

$$S_I = \frac{K^3 h^4}{4} \left( \frac{3n+2}{n} G^2 - \frac{4n+4}{n(n-1)} BG + \frac{n+2}{(n-1)^2 n} B^2 + \frac{n^2}{(n-1)^2} \right), \quad (3.3)$$

$$S_{II} = \frac{HK^2 h^2}{2} \left( \frac{2n+1}{n} G - \frac{n+1}{n(n-1)} B \right), \quad (3.4)$$

$$S_{III} = H^2 K, \quad (3.5)$$

$$S_{IV} = \frac{H^2 K}{n}, \quad (3.6)$$

$$S_V = 0, \quad (3.7)$$

where  $h$  is the marginal ray height,  $B$  is shape factor of the lens,  $n$  is the refractive index of the material assigned to the lens,  $G$  is the conjugate factor of the lens,  $K$  is the optical power of the lens,  $H$  is the Lagrange invariant of the optical system [22]. Seidel sums in Eqs. 3.3 - 3.7 represent the well-known primary optical aberrations consecutively, which are spherical aberration, coma, astigmatism, field curvature and distortion. Shape factors and conjugate factors are defined according to the radius of curvatures of the lens and its ray trace parameters as follows:

$$B = \frac{c_1 + c_2}{c_1 - c_2}, \quad (3.8)$$

$$G = \frac{u + u'}{u - u'}, \quad (3.9)$$

where curvatures of the lens are  $c_1$  and  $c_2$ , the angle of the marginal ray which enters and leaves the lens with respect to the optical axis are given by  $u$  and  $u'$ . Since the stop position in an optical system can not be at all of the paraxial lenses in an optical design, Seidel sums given by Eqs. 3.3 - 3.7 must be extended such that they are also valid when stop is shifted with respect to a paraxial lens. Hence, stop shift equivalents of the Seidel sums are given as follows [3]:

$$S_I^* = S_I, \quad (3.10)$$

$$S_{II}^* = S_{II} + \frac{\bar{h}}{h} S_I, \quad (3.11)$$

$$S_{III}^* = S_{III} + 2 \frac{\bar{h}}{h} S_{II} + \left( \frac{\bar{h}}{h} \right)^2 S_I, \quad (3.12)$$

$$S_{IV}^* = S_{IV}, \quad (3.13)$$

$$S_V^* = S_V + \frac{\bar{h}}{h} (3S_{III} + S_{IV}) + 3 \left( \frac{\bar{h}}{h} \right)^2 S_{II} + \left( \frac{\bar{h}}{h} \right)^3 S_I. \quad (3.14)$$

Table 3.1: Algebraic and vectorial notation of optical aberration [2].

Aberration name	Vector form	Algebraic form	j	m	n
<b>Zero order</b>					
Uniform piston	$W_{000}$	$W_{000}$	0	0	0
<b>Second order</b>					
Quadratic piston	$W_{200}(\vec{H} \cdot \vec{H})$	$W_{200}H^2$	1	0	0
Magnification	$W_{111}(\vec{H} \cdot \vec{\rho})$	$W_{111}H\rho \cos(\phi)$	0	1	0
Focus	$W_{020}(\vec{\rho} \cdot \vec{\rho})$	$W_{020}H\rho^2$	0	0	1
<b>Fourth order</b>					
Spherical aberration	$W_{040}(\vec{\rho} \cdot \vec{\rho})^2$	$W_{040}\rho^4$	0	0	2
Coma	$W_{131}(\vec{H} \cdot \vec{\rho})(\vec{\rho} \cdot \vec{\rho})$	$W_{131}H\rho^3 \cos(\phi)$	0	1	1
Astigmatism	$W_{222}(\vec{H} \cdot \vec{\rho})^2$	$W_{222}H^2\rho^2 \cos^2(\phi)$	0	2	0
Field curvature	$W_{220}(\vec{H} \cdot \vec{H})(\vec{\rho} \cdot \vec{\rho})$	$W_{220}H^2\rho^2$	1	0	1
Distortion	$W_{311}(\vec{H} \cdot \vec{H})(\vec{H} \cdot \vec{\rho})$	$W_{311}H^3\rho \cos(\phi)$	1	1	0
Quartic piston	$W_{400}(\vec{H} \cdot \vec{H})^2$	$W_{400}H^4$	2	0	0
<b>Sixth order</b>					
Oblique spherical aber.	$W_{240}(\vec{H} \cdot \vec{H})(\vec{\rho} \cdot \vec{\rho})^2$	$W_{240}H^2\rho^4$	1	0	2
Coma	$W_{331}(\vec{H} \cdot \vec{H})(\vec{H} \cdot \vec{\rho})(\vec{\rho} \cdot \vec{\rho})$	$W_{331}H^3\rho^3 \cos(\phi)$	1	1	1
Astigmatism	$W_{422}(\vec{H} \cdot \vec{H})(\vec{H} \cdot \vec{\rho})^2$	$W_{422}H^4\rho^2 \cos^2(\phi)$	1	2	0
Field curvature	$W_{420}(\vec{H} \cdot \vec{H})^2(\vec{\rho} \cdot \vec{\rho})$	$W_{420}H^4\rho^2$	2	0	1
Distortion	$W_{511}(\vec{H} \cdot \vec{H})^2(\vec{H} \cdot \vec{\rho})$	$W_{511}H^5\rho \cos(\phi)$	2	1	0
Piston	$W_{600}(\vec{H} \cdot \vec{H})^3$	$W_{600}H^6$	3	0	0
Spherical aberration	$W_{060}(\vec{\rho} \cdot \vec{\rho})^3$	$W_{060}\rho^6$	0	0	3
Unnamed	$W_{151}(\vec{H} \cdot \vec{\rho})(\vec{\rho} \cdot \vec{\rho})^2$	$W_{151}H\rho^5 \cos(\phi)$	0	1	2
Unnamed	$W_{242}(\vec{H} \cdot \vec{\rho})^2(\vec{\rho} \cdot \vec{\rho})$	$W_{242}H^2\rho^4 \cos^2(\phi)$	0	2	1
Unnamed	$W_{333}(\vec{H} \cdot \vec{\rho})^3$	$W_{333}H^3\rho^3 \cos^3(\phi)$	0	3	0

where  $\bar{h}$  is the chief ray height.

Abovementioned Seidel sum equations are monochromatic which means that they are valid for only a defined operating wavelength. Since infrared imaging systems are designed in a broadband wavelength region, in order to gather radiation from

the target as much as possible, chromatic aberrations must also be controlled in an infrared lens. Chromatic aberration coefficients are given as follows:

$$C_I = \sum_{i=1}^n \frac{h_i^2 K_i}{V_i}, \quad (3.15)$$

$$C_{II} = \sum_{i=1}^n \frac{h_i \bar{h}_i K_i}{V_i}, \quad (3.16)$$

where  $n_i$  is the refractive index of the  $i$ 'th lens,  $V_i$  is the Abbe number of the  $i$ 'th lens,  $\bar{h}_i$  is the chief ray height at the  $i$ 'th lens,  $K_i$  is the optical power of the  $i$ 'th lens.

Categorizing optical aberrations as shape dependent and shape independent is very important in systematic way of designing lenses. As can be seen from the general structure of aberration equations, axial colour ( $C_I$ ), lateral colour ( $C_{II}$ ) and field curvature ( $S_{IV}$ ) do not depend on the shape factors of the lenses. Similar to shape independent aberrations, focal length of the lens does not depend on shapes of the lenses. Optical power of a lens is calculated with the scale equation which is given by:

$$K = \sum_{i=1}^n \frac{h_i}{h_1} K_i, \quad (3.17)$$

where  $h_i$  is the marginal ray height at the  $i$ 'th lens,  $h_1$  is the marginal ray height at the first lens,  $K_i$  is the optical power of the  $i$ 'th lens and  $K$  is the effective optical power of the total system [3]. However, spherical aberration ( $S_I$ ), coma ( $S_{II}$ ), astigmatism ( $S_{III}$ ) and distortion ( $S_V$ ) depend on the shape factor of the lens. Lens powers and shapes are the most effective parameters in correcting aberrations in an optical design. It is very important to correct shape independent aberrations in paraxial form of the design and then correct the shape dependent aberrations. If shape independent aberrations are not corrected conveniently in paraxial form and materials and power distributions of lenses are determined without concerning about the shape independent aberrations, it is very hard to correct them in later stages of the optical design.

Seidel sums are very useful equations in optical design which enables to transform ideal paraxial optical designs, in which first order optical parameters namely the optical specifications are satisfied, into real lenses with third order primary aberration correction. This method gives promising starting points for further aberration balancing based optimizations in lens design. Although very powerful computers are relatively easily reachable and can generate different optical solutions without deep

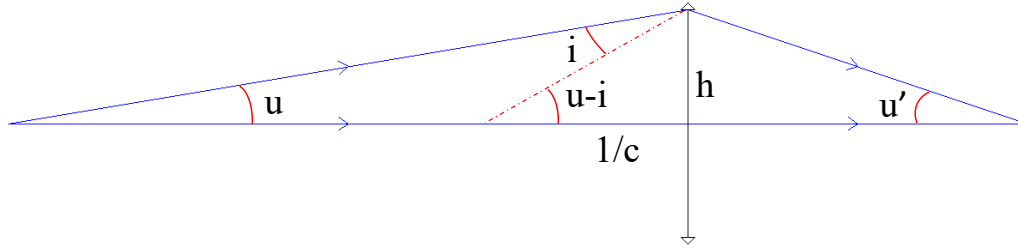


Figure 3.5: Marginal ray trace.

optical knowledge, understanding and controlling optical aberrations are still very important in optical lens design in order to find a superior solution in design hyperspace [23, 24].

### 3.2 Thin Lens Narcissus Model Derivation

At the beginning of the optical lens design, namely the layout and thin-lens pre-design stages, narcissus performance of infrared lenses is not involved in calculations because of the fact that all of the lenses are in their paraxial forms. In order to include narcissus performance in early design stages, a connection between the optical parameters in Seidel sum equations, which are shape factor, conjugate factor and optical powers, and conventional narcissus control parameters which are  $i / \bar{i}$  and  $yni$  must be constructed. If conventional narcissus control parameters are expressed in terms of paraxial lens parameters, and two narcissus metrics are derived similar to third order aberration coefficients, narcissus performance of the infrared lens can be taken into account in the early design stages.

Initially, paraxial parameters of narcissus control parameters which are  $i$  and  $\bar{i}$  have to be expressed in terms of paraxial lens optical parameters which are  $B$ ,  $G$ ,  $K$  and  $H$ . A marginal raytrace of a typical thin lens is shown in Fig. 3.5.

The relation between marginal ray angle with respect to surface normal ( $i$ ), surface curvature ( $c$ ), marginal ray height ( $h$ ) and marginal ray angle with respect to optical

axis ( $u$ ) can be expressed with the help of Fig. 3.5 as follows:

$$i = u + hc \quad , \quad (3.18)$$

$$\bar{i} = \bar{u} + \bar{h}c \quad . \quad (3.19)$$

Optical power of a thin lens ( $K$ ) and Lagrange invariant ( $H$ ) are given as follows:

$$H = n(h\bar{u} - u\bar{h}), \quad (3.20)$$

$$K = (n - 1)(c_1 - c_2). \quad (3.21)$$

When Eqs. 3.8 and 3.21 are solved together, radius of curvatures of thin lens are found as follows:

$$c_1 = \frac{K}{2} \left( \frac{B + 1}{n - 1} \right), \quad (3.22)$$

$$c_2 = \frac{K}{2} \left( \frac{B - 1}{n - 1} \right). \quad (3.23)$$

If  $c_1$  and  $c_2$  are put in Eqs. 3.18 and 3.19,  $i$  and  $\bar{i}$  are found as follows:

$$i_1 = u + h \frac{K}{2} \left( \frac{B + 1}{n - 1} \right), \quad (3.24)$$

$$i_2 = u' + h \frac{K}{2} \left( \frac{B - 1}{n - 1} \right), \quad (3.25)$$

$$\bar{i}_1 = \bar{u} + \bar{h} \frac{K}{2} \left( \frac{B + 1}{n - 1} \right), \quad (3.26)$$

$$\bar{i}_2 = \bar{u}' + \bar{h} \frac{K}{2} \left( \frac{B - 1}{n - 1} \right). \quad (3.27)$$

Imaging condition for a thin lens is given as

$$u = u' + hK \quad . \quad (3.28)$$

Solving Eqs. 3.9 and 3.28 together,  $u$  and  $u'$  are found:

$$u = \frac{hK}{2}(G + 1), \quad (3.29)$$

$$u' = \frac{hK}{2}(G - 1). \quad (3.30)$$

When Eqs. 3.29 and 3.30 are put in Eqs. 3.24 and 3.25, respectively,  $i$  is expressed as

$$i_1 = \frac{hK}{2} \left( G + 1 + \frac{B + 1}{n - 1} \right), \quad (3.31)$$

$$i_2 = \frac{hK}{2} \left( G - 1 + \frac{B - 1}{n - 1} \right). \quad (3.32)$$

$yni$  which is the first conventional paraxial narcissus control parameter, can now be used for a paraxial lens in thin lens predesign stage.

In order to transform second narcissus control parameter,  $i/\bar{i}$ , such that it can be used for paraxial lens in thin lens predesign stage, further derivations are necessary.

When Eqs. 3.20, 3.29 and 3.30 are solved together,  $\bar{u}$  and  $\bar{u}'$  are found as

$$\bar{u} = \frac{\bar{h}}{h}u + \frac{H}{h} = \frac{\bar{h}K}{2}(G + 1) + \frac{H}{h} \quad , \quad (3.33)$$

$$\bar{u}' = \frac{\bar{h}}{h}u' + \frac{H}{h} = \frac{\bar{h}K}{2}(G - 1) + \frac{H}{h} \quad . \quad (3.34)$$

When Eqs. 3.33 and 3.34 are put in Eqs. 3.26 and 3.27,  $\bar{i}_1$  and  $\bar{i}_2$  are found as

$$\bar{i}_1 = \frac{\bar{h}K}{2} \left( G + 1 + \frac{B + 1}{n - 1} \right) + \frac{H}{h} \quad , \quad (3.35)$$

$$\bar{i}_2 = \frac{\bar{h}K}{2} \left( G - 1 + \frac{B - 1}{n - 1} \right) + \frac{H}{h} \quad . \quad (3.36)$$

As a summary, conventional narcissus control parameters are expressed in terms of paraxial lens optical parameters which are used in thin lens predesign stages which are  $B$ ,  $G$ ,  $H$  and  $K$ . It is now possible to include narcissus performance in early design stages of infrared lenses by using these expressions which are given as

$$yni_1 = \frac{h^2K}{2} \left( G + 1 + \frac{B + 1}{n - 1} \right) \quad , \quad (3.37)$$

$$yni_2 = \frac{h^2K}{2} \left( G - 1 + \frac{B - 1}{n - 1} \right) \quad , \quad (3.38)$$

$$\left( \frac{i}{\bar{i}} \right)_1 = \frac{\frac{hK}{2} \left( G + 1 + \frac{B+1}{n-1} \right)}{\frac{\bar{h}K}{2} \left( G + 1 + \frac{B+1}{n-1} \right) + \frac{H}{h}} \quad , \quad (3.39)$$

$$\left( \frac{i}{\bar{i}} \right)_2 = \frac{\frac{hK}{2} \left( G - 1 + \frac{B-1}{n-1} \right)}{\frac{\bar{h}K}{2} \left( G - 1 + \frac{B-1}{n-1} \right) + \frac{H}{h}} \quad . \quad (3.40)$$

In an infrared lens design, narcissus effect is controlled by four parameters for each lens. Reciprocals of these parameters are proposed because of the fact that the greater these narcissus control parameters are, the better the narcissus performance is. RMS of reciprocals of these parameters are proposed as narcissus metrics in this work. Hence, as the proposed narcissus metrics approach to zero, narcissus performance of the lens gets better. Finally, narcissus metrics which can be utilized in early paraxial

lens design stage are derived as

$$N_I = \left\{ \frac{1}{T} \sum_{m=1}^T \left[ \frac{h^2 K}{2} \left( G + (-1)^{m+1} + \frac{B + (-1)^{m+1}}{n-1} \right) \right]^{-2} \right\}^{1/2}, \quad (3.41)$$

$$N_{II} = \left\{ \frac{1}{T} \sum_{m=1}^T \left[ \frac{\frac{hK}{2} \left( G + (-1)^{m+1} + \frac{B+(-1)^{m+1}}{n-1} \right)}{\frac{\bar{h}K}{2} \left( G + (-1)^{m+1} + \frac{B+(-1)^{m+1}}{n-1} \right) + \frac{H}{h}} \right]^{-2} \right\}^{1/2}. \quad (3.42)$$

where T is the total number of optical surfaces in an infrared lens [25].





## CHAPTER 4

### APPLICATION OF THE THIN LENS NARCISSUS MODEL

#### 4.1 Specifications and Paraxial Layout

There are two very useful operating wavelength bands for observing infrared radiation in military systems. These two bands are determined by atmosphere through which majority of military infrared systems gather radiation from targets. A typical transmission of atmosphere is given in Fig. 4.1 [6]. As shown in the figure, majority of the band is absorbed by  $CO_2$  and  $H_2O$  gases. Transmission band between 3-5 $\mu\text{m}$  is called mid-wave infrared (MWIR) band and between 8-12 $\mu\text{m}$  is called long-wave infrared (LWIR). A fictitious infrared lens system which operates in LWIR band is

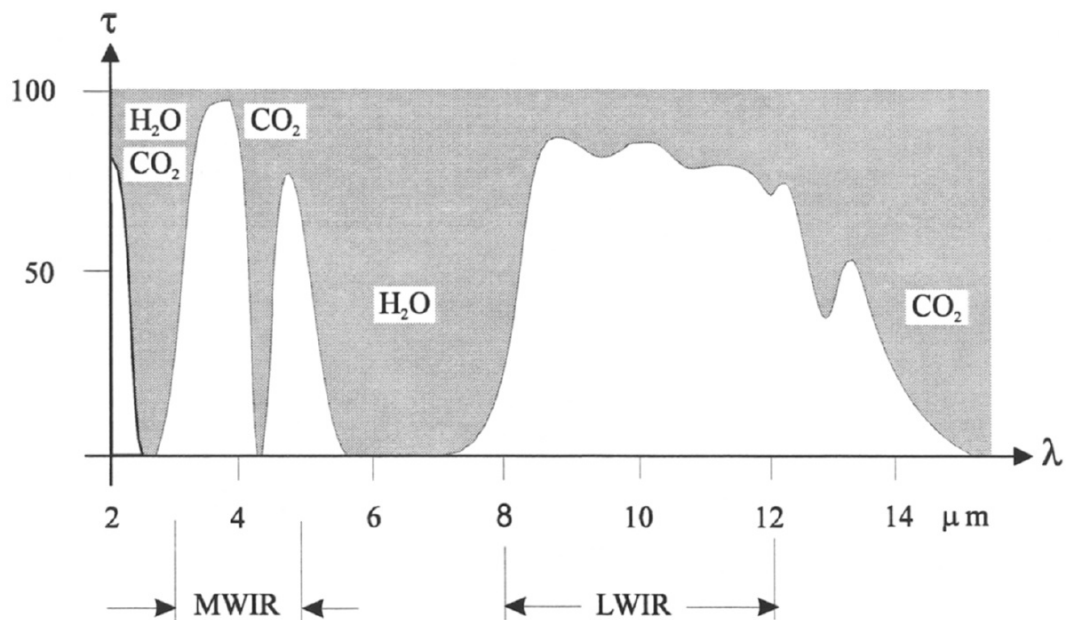


Figure 4.1: Atmospheric windows in infrared [6].

Table 4.1: Specifications of the LWIR application used in this thesis.

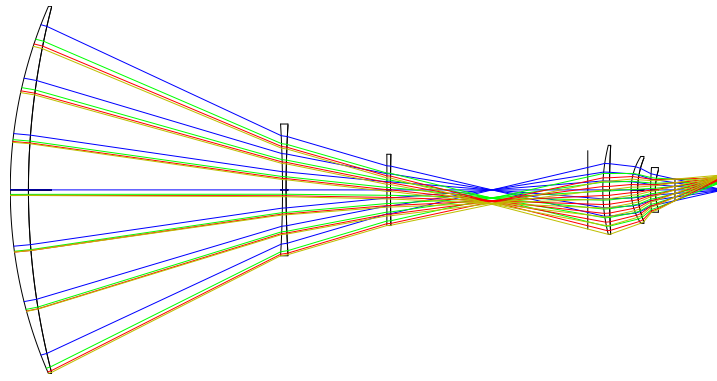
$f_{\#}$	2.25
Detector pixels	$640 \times 512$
Detector pixel size	$15 \mu\text{m}$
Detector Sensitivity (NETD)	25-30 mK
Cold stop height	20.4 mm
Operating wavelength	$7.7\text{-}9.3 \mu\text{m}$
Focal length	325 mm
Field of view (horizontal)	$1.69^{\circ}$

designed with the help of proposed narcissus model starting from scratch. General lens design steps followed are given as follows:

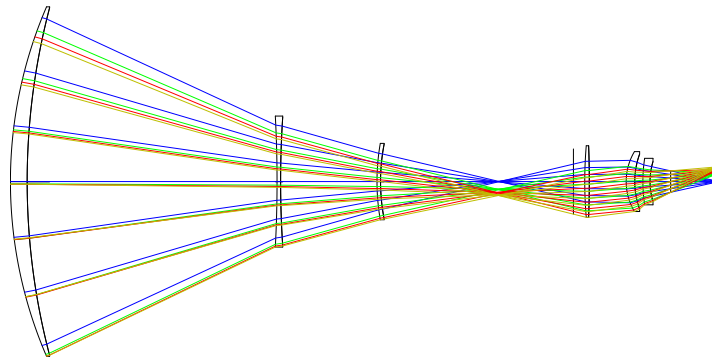
1. An optical architecture is chosen and paraxial form of the lens is designed. Optical materials and powers are determined in order to correct the shape independent aberrations.
2. Lens shape factors are optimized such that shape dependent aberrations are corrected.
3. Thicknesses are introduced to the thin lenses in order for them to carry optical power.
4. Computational power is used in order to search for a better configuration with the help of aberration balancing.

For the application studied in this work, targeted optical specifications are given in Table 4.1. Optical system is specified to operate at a relatively fast speed of  $f_{\#}/2.25$ . Focal length is defined to be 325 mm. Operating wavelength is in LWIR which is limited to  $7.7\text{--}9.3 \mu\text{m}$ . The detector has  $640 \times 512$  format with  $15 \mu\text{m}$  pixel size. Sensitivity of the detector is 25-30 mK. Position of the cold stop from the FPA is given as 20.4 mm.

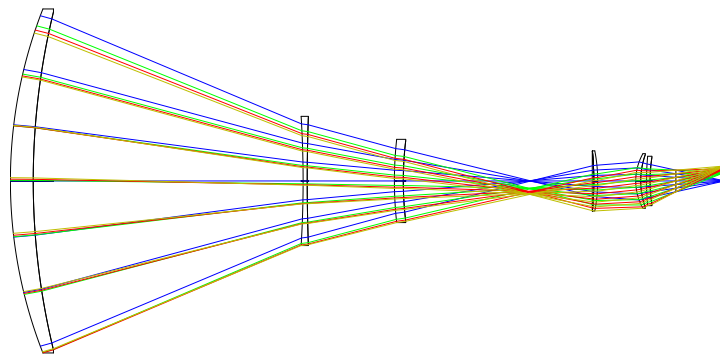
First, three optical designs are generated by computerized design methods in which aberration theory and proposed narcissus model are not utilized. Layouts of these



(a)



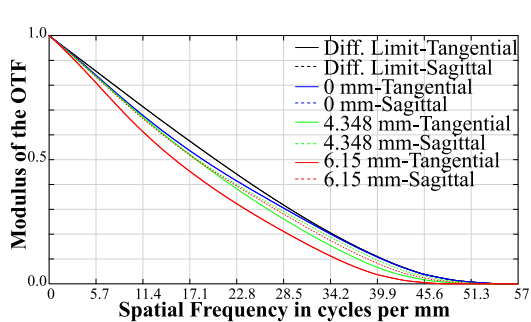
(b)



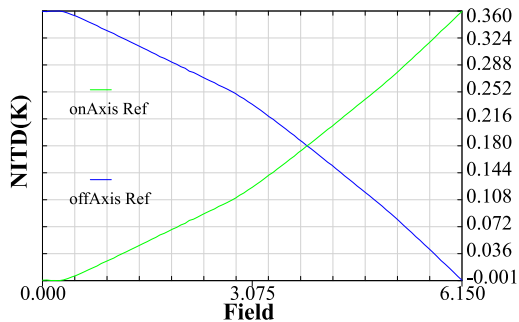
(c)

Figure 4.2: Optical layouts designed with computerized methods: (a) design 1, (b) design 2, (c) design 3.

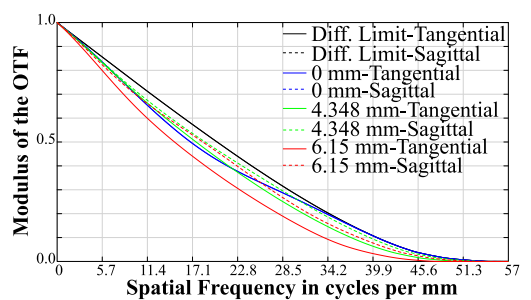
designs are given in Fig. 4.2. Imaging quality performance in terms of MTF and narcissus performance in terms of NITD of these design sets are given in Fig. 4.3.



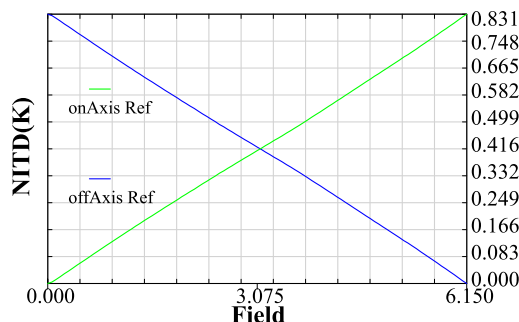
(a) Polychromatic diffraction MTF



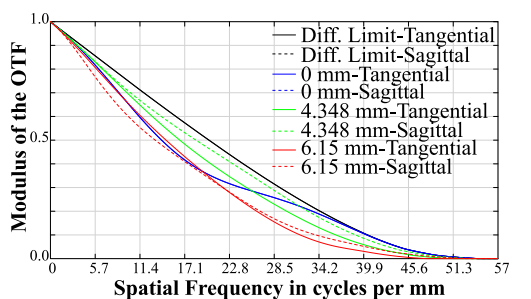
(b) Total NITD



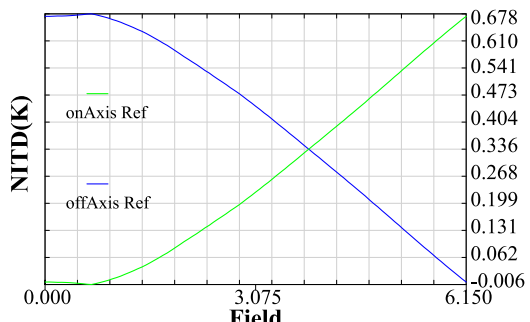
(c) Polychromatic diffraction MTF



(d) Total NITD



(e) Polychromatic diffraction MTF



(f) Total NITD

Figure 4.3: MTF and Narcissus performances of optical layouts designed with computerized methods: (a) design 1 MTF, (b) design 1 Narcissus, (c) design 2 MTF, (d) design 2 Narcissus, (e) design 3 MTF, (f) design 3 Narcissus

Although MTF performances of design 1, 2 and 3 are very close to each other and are very close to diffraction limit, they have a wide range of narcissus performance. NITD values of these designs vary from 0.360 K to 0.831 K which are totally unacceptable.

A systematic way of lens design in which both optical imaging quality and narcissus performances are considered in early design stage is necessary. In order to satisfy first order parameters of infrared lens which are focal length,  $f\#$  and field of view, an appropriate optical architecture is chosen in this step. Since the physical stop must be cooled and positioned inside the detector cooler, there is no control of stop position in infrared systems with cooled detectors. As a results, in order to limit the diameter of the first lens which is the largest and the most expensive one, cold stop must be projected to the position of the first lens with the help of an internal image plane. Hence, an optical architecture which has a front focuser objective and a relay group is chosen for this example. After selecting optical architecture, lens numbers in each subgroup must be determined. Different lens number combinations could be used depending on the number of constraints in the optical system. In this example, 3 lenses for each group in the optical architecture are chosen which is sufficient to control both optical aberrations and narcissus performance. By using scale equation (Eq. 3.17), field curvature (Eq. 3.6), axial and lateral color equations (Eqs. 3.15 - 3.16), materials, positions and powers of paraxial lenses which form the LWIR objective are determined. Variables in this architecture with the chosen lens numbers are as follows: six material, six air thickness and six optical power. Scale equation, axial color, lateral color and field curvature equations are solved with the cold stop projection constraint by optimizing these optical variables. Trial and error method is used for determining initial values of these variables. With the help of composite merit function operands in ZEMAX, all of the aforementioned equations are implemented and solved using Damped Least Squares (DLS) optimization algorithm in ZEMAX. The great benefit of this approach to lens design is that all of these equations can be constructed by tracing only two ray namely marginal and chief ray in an optical system in linear domain. Time consuming optimization with increased number of rays which is necessary to sample the optical system sufficiently is not needed. After the proposed architecture is optimized, parameters of the optical design are given in Table 4.2 and optical layout is shown in Fig. 4.4.

It is important to emphasize that in infrared systems with cooled detectors, since physical stop is inside the dewar assembly, designing the lens starting from the detector FPA plane to the environment increases the efficiency of ray tracing algorithms.

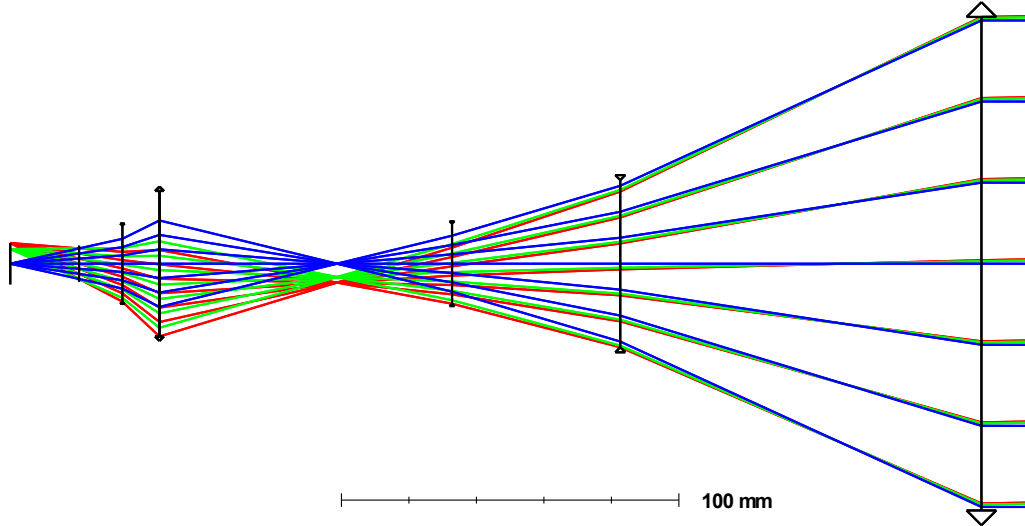


Figure 4.4: Paraxial layout of the LWIR application.

Hence, reversed design technique is used throughout this work.

The optical layout which is achieved by targeting shape independent aberrations which are field curvature ( $S_{IV}$ ), axial color ( $C_I$ ) and lateral color ( $C_{II}$ ) is shown in Fig. 4.4. As given in Table 4.3 (shape independent aberration), designed optical layout has sufficient shape independent aberration performance. At this stage, only first order optical parameters namely optical specifications and shape independent aberrations are taken into account. Shape factors of the lenses are not used at this stage, consequently proposed narcissus model is not utilized. Since optical powers, materials and positions of lenses which form the optical system are assigned and shape independent aberrations are sufficiently corrected, shape dependent aberrations namely spherical aberration ( $S_I$ ), coma ( $S_{II}$ ), astigmatism ( $S_{III}$ ) and distortion ( $S_V$ ) with narcissus ( $N_I, N_{II}$ ) metrics of the lens can now be targeted. At the next stage which is the shape factor optimization, proposed narcissus model will be applied in order to consider narcissus performance of the optical lens.

## 4.2 Shape Factor Optimization

In the previous optical layout stage, a suitable lens architecture is chosen according to the optical specifications defined. According to the optical architecture chosen,

Table 4.2: Lens data of the LWIR application used in this thesis.

Surface	Comment	Type	Thickness	Semi-Diameter	Focal length	Material
OBJ	Detector FPA	Standart	20.4	6.15	-	-
STO	Cold Stop	Standart	12.856	4.533	-	-
2	Lens 1	Paraxial	11	11.265	-27.106	ZincSelenide
3	Lens 2	Paraxial	0	21.597	30.291	Germanium
4	Lens 3	Paraxial	86.777	21.597	40.748	Germanium
5	Lens 4	Paraxial	49.901	11.878	-157.215	Germanium
6	Lens 5	Paraxial	107.129	24.818	-143.105	ZincSelenide
7	Lens 6	Paraxial	15	73.256	157.589	Germanium
IMA	Environment	Standart	0	73.540	-	-

lens numbers, optical powers, materials and positions are determined such that the shape independent aberrations are corrected and optical focal length is satisfied with the help of ZEMAX DLS optimization algorithm by solving Eqs. 3.6, 3.15, 3.16 and 3.17. Optical lenses have now a sufficient shape independent aberration ( $S_{IV}$ ,  $C_I$ ,  $C_{II}$ ) performance with the specified optical power ( $K$ ). Optical design is still in its paraxial form. In order to make lenses physical, shape factors of the lenses must be assigned to lenses such that shape dependent aberrations which are given by Eqs. 3.3 - 3.7 and Eqs. 3.10 - 3.14 are corrected sufficiently. This is the place where proposed narcissus model which is constructed on Eqs. 3.41 and 3.42 is included into optical design stages. All of the necessary optical parameters which appear in the shape dependent aberrations and narcissus metrics equations are available and given in Table 4.2. It is now possible to solve these equations and calculate shape factors of lenses with the help of composite merit function operands in ZEMAX and utilize DLS optimization algorithm in ZEMAX. The paraxial form of the optical lens is not changed at this stage. Since paraxial form is already optimized in layout stage, ray tracing based optimization is not needed at this stage. Only shape factors are optimized according to the shape dependent aberrations and narcissus equations. Hence, optimization is much faster than ray-based optimization in ZEMAX. Shape factor optimization is not strictly restricted to an optical software which is capable of raytracing and optimization since ray tracing is not needed at this stage. Other softwares having

Table 4.3: Seidel coefficients of the LWIR application. Leftmost two columns represent shape independent aberrations and rightmost two columns represent shape dependent aberrations with narcissus metrics of the LWIR application.

Shape Independent Aberrations		Shape Dependent Aberrations	
Type	Coefficient	Type	Coefficient
$S_{IV}$ (field curvature)	-0.007111	$S_I$ (spherical aberration)	0.09854851
$C_I$ (axial color)	-0.002552	$S_{II}$ (coma)	0.00887242
$C_{II}$ (lateral color)	0.000673	$S_{III}$ (astigmatism)	0.00629927
		$S_V$ (distortion)	0.08306280
		Narcissus Metrics	
		$N_I$	0.4510510
		$N_{II}$	0.6957296

optimization capability could also be used at this stage. Since shape dependent aberration equations with narcissus equations are highly complex, analytical solutions to these equations are not attempted in this work. At the end of this stage, shape factors of lenses are found and given in Table 4.4. Narcissus metrics with shape dependent aberrations according to the found shape factors are also calculated and given in Table 4.3 (last two columns). Since shape factors of lenses are now found, it is possible to calculate narcissus control parameters for each surface of lenses forming the optical system. Conventional paraxial narcissus control parameters which are  $yni$  and  $i/\bar{i}$  are calculated and given in Table 4.4. Majority of these narcissus control parameters are greater than unity which means a satisfactory narcissus performance is expected from the designed optical system.

### 4.3 Real Thin Lens Layout and Narcissus Performance

In shape factor optimization stage, shape factors of the lenses are optimized such that shape dependent aberrations are corrected and narcissus performance of the optical system is taken into account. Since shape factors of the lenses are known, paraxial lenses can now be transformed into real lenses with zero center thickness. Curvatures



Table 4.4: Results of the LWIR application for the proposed narcissus model. Subscripts 1 and 2 refer to the surfaces on the detector side and on the scene side, respectively.

Lens	$B$	$yni_1$	$yni_2$	$\left(\frac{i}{i}\right)_1$	$\left(\frac{i}{i}\right)_2$
1	4.1068	28.1110	-15.9923	-29.2207	10.0158
2	-0.0684	-11.8268	-5.4493	23.6567	5.6338
3	-6.7228	-2.0491	-1.4624	4.1813	1.9735
4	-1.2626	2.9515	-2.4344	4.5456	0.8036
5	5.7623	5.2018	-2.0435	2.3793	0.7398
6	-2.7410	-2.4171	1.0214	0.9176	-1.2294

of the lenses are calculated by Eq. 3.22 and Eq. 3.23. Optical layout with real thin lenses is shown in Fig. 4.5 and optical prescription data is given in Table 4.5.

Up to this stage of optical design, all of the optical performances are considered with the help of Seidel coefficients and proposed narcissus metrics in order to simplify optical design and design lenses in a systematic way. However, only Seidel coefficients and narcissus metrics are not sufficient to estimate the final optical performance of the optical lens although they give useful and strong initial points for optical lenses for

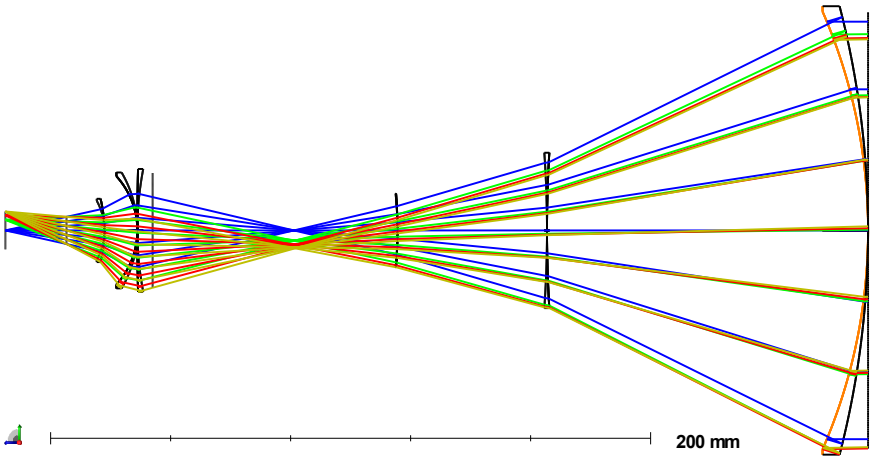


Figure 4.5: Optical layout of the LWIR application with real thin lenses.

Table 4.5: Lens data of the LWIR application after transforming paraxial lenses into real lenses.

	Surf : Type	Radius	Thickness	Glass	Semi-Diameter
OBJ	Standart	$\infty$	20.400		6.150
1	Standart	$\infty$	12.630		4.533
2	Standart	-20.502	0	ZincSelenide	9.835
3	Standart	-44.055	11		10.502
4	Standart	-38.240	0	Germanium	19.226
5	Standart	-26.930	0		18.009
6	Standart	108.273	0	Germanium	20.209
7	Standart	932.799	86.778		20.384
8	Standart	-122.389	0	Germanium	12.194
9	Standart	-165.162	49.901		12.213
10	Standart	-378.981	0	ZincSelenide	25.678
11	Standart	434.698	107.130		25.926
12	Standart	-299.746	0	Germanium	74.884
13	Standart	-183.583	0		73.096
IMA	Standart	$\infty$	0		72.865

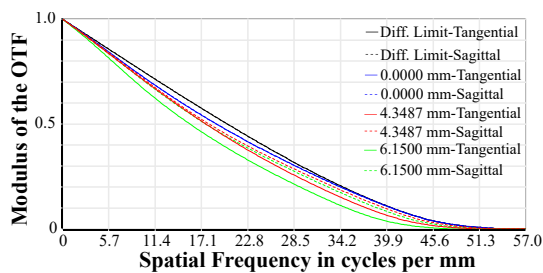
further optimizations. Two of the image quality assessment criteria in optical design are spot size and MTF. In order to assess real optical performance of optical system which is composed of zero thickness real lenses, MTF and spot size performance routines which are based on real ray tracing in ZEMAX are used. Spot distribution and MTF of the optical design for LWIR application are given in Fig. 4.6. MTF and spot size distribution show that proposed initial solution for the LWIR application has nearly diffraction limited performance from aberration perspective.

Similar to optical aberration performance, narcissus performance of the optical lens is considered in an indirect way with the proposed narcissus metrics. In order to assess final narcissus performance of an infrared lens with cooled detectors, total narcissus distribution across the FPA must be analysed. In order to analyse narcissus

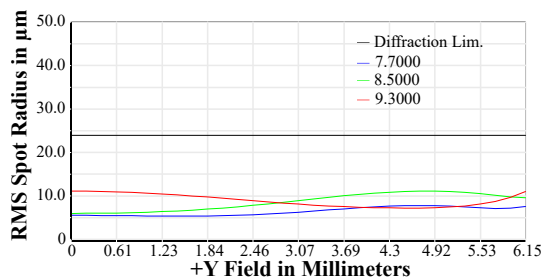
distribution at the FPA, exact ray tracing techniques are applied after optical design is finished [26, 27]. Narcissus distribution in an infrared lens is analysed in ZEMAX platform with the help of a macro coded in ZPL based on exact ray tracing algorithms [10]. Iteratively, single bounce ghost files are generated for each surface of the lens in the optical system. Each surface's cold return values are calculated in corresponding single bounce file with the help of vignetting routine in ZEMAX. Afterwards, Eq. 2.6 is applied in half diagonal direction of the FPA in order to get the total narcissus distribution at the detector plane. Narcissus distribution of the LWIR application is shown in Fig. 4.6. Anti-reflective coating's reflection is taken as uniform 0.3% and transmission is taken as uniform 99%. Temperatures are assigned 300 K for housing and scene, 77 K for cooled detector. According to the real ray-trace based narcissus analysis, NITD of the designed LWIR infrared lens is around 18-19 mK. Noise Equivalent Temperature Difference (NETD) performances of the off-the-shelf LWIR detectors are around 25-30 mK [28, 29]. Since magnitude of the narcissus image at the detector plane across all over the FPA is much smaller than the sensitivity of the detector, image degradation due to the unwanted narcissus effect can not be detected by the detector. As a design rule of thumb, it is advisable to reduce total narcissus contribution in an infrared lens with cooled detectors below to the minimum detectable temperature difference levels of the detectors to be used in infrared optical system.

#### **4.4 Real Thick Lens Layout and Narcissus Performance**

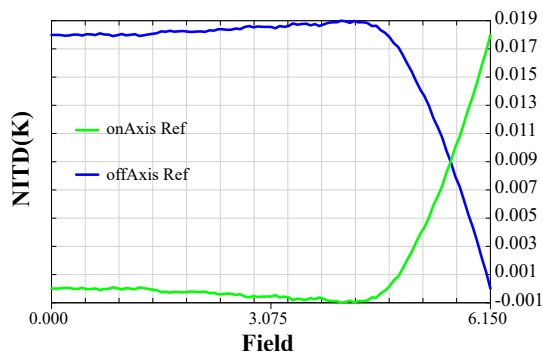
In previous stages, optical architecture which is suitable to the optical specifications is chosen. According to the optical architecture, lens numbers, powers and materials are determined such that shape independent aberrations are corrected satisfying the focal length. Then, paraxial lenses are transformed into real lenses by optimizing shape factors such that shape dependent aberrations are corrected and narcissus performance is under control. Aberration performance and narcissus performance are shown to be satisfactory with exact ray tracing methods. Although paraxial lenses are transformed into real lenses, optical system is still non-physical at this stage since lenses do not have center thickness in order to carry optical power. In order for lenses to carry



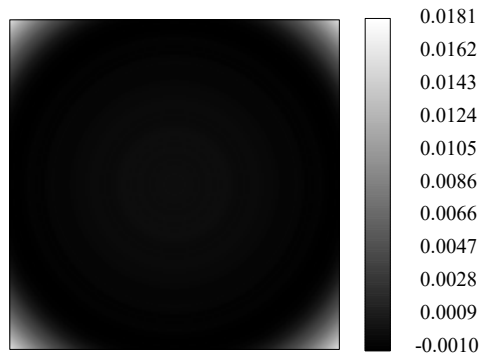
(a) Polychromatic Diffraction MTF.



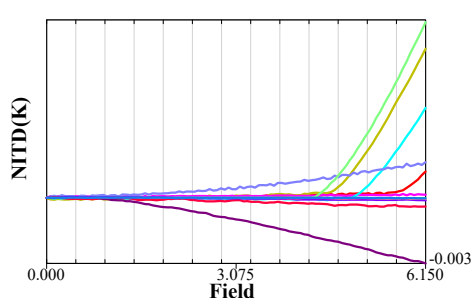
(b) RMS Spot Radius vs Field.



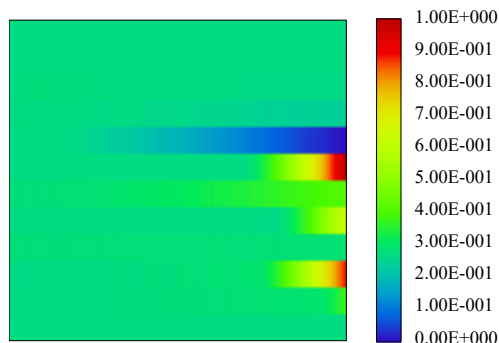
(c) Total NITD.



(d) 2D Narcissus Image.



(e) Surface Narcissus Contributions.



(f) 2D surface contributions.

Figure 4.6: Optical performance (a, b) and Narcissus performance (c, d, e, f) of the LWIR application with real thin lenses.

optical power, center thicknesses must be introduced to the lenses. A few cycles of optimization routines are utilized in order to increase thicknesses of lenses. Generally, aberration balance and narcissus performance of an optical system are not affected by the center thickness of a lens. After thicknesses are introduced to the lenses forming LWIR system, optical layout shown in Fig. 4.7 is achieved. Prescription data of the

Table 4.6: Lens data of the LWIR application after lenses are thickened.

	Surf:Type	Radius	Thickness	Glass	Semi-Diameter
OBJ	Standart	$\infty$	20.400		6.150
1	Standart	$\infty$	12.684		4.533
2	Standart	-20.542	1.5	ZincSelenide	9.857
3	Standart	-45.678	6.848		11.259
4	Standart	-35.659	3.103	Germanium	16.364
5	Standart	-26.963	0.572		17.025
6	Standart	95.596	2.750	Germanium	18.997
7	Standart	459.325	89.594		18.877
8	Standart	-214.434	1.5	Germanium	13.927
9	Standart	-330.050	43.226		14.090
10	Standart	-502.121	1.5	ZincSelenide	25.855
11	Standart	435.405	107.142		26.274
12	Standart	-311.710	7.087	Germanium	72.814
13	Standart	-194.662	0		73.234
IMA	Standart	$\infty$	0		73.016

optical layout is given in Table 4.6. A very slight change is observed in optical layout after thickness introduction, nevertheless final optical performance of the design must

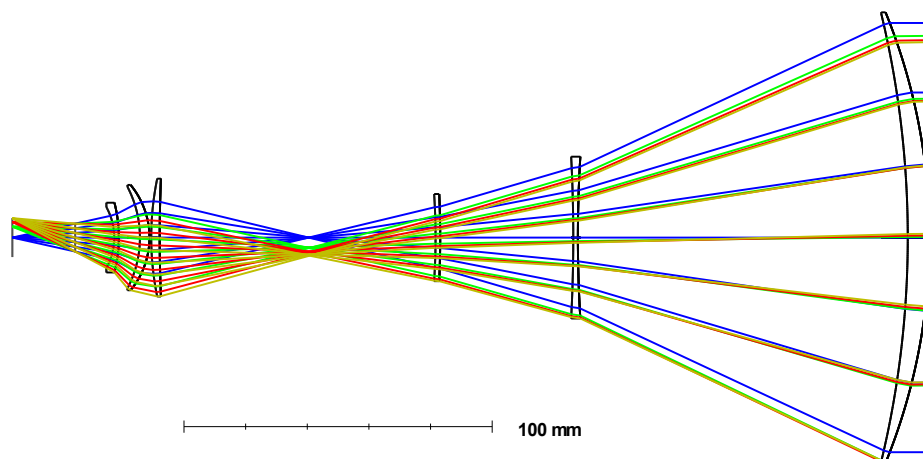
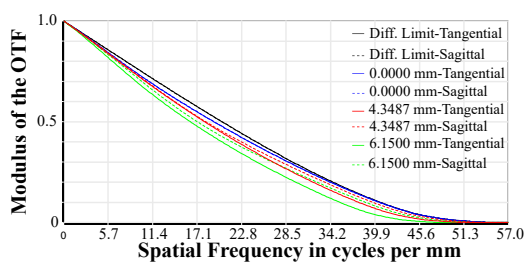
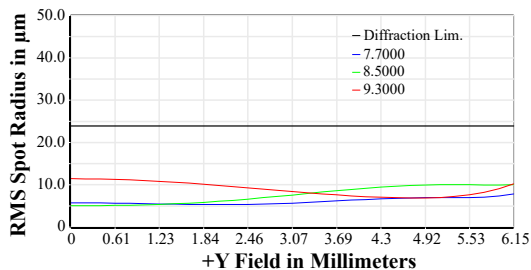


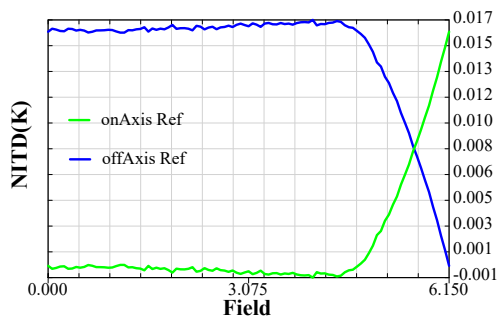
Figure 4.7: Optical layout of the LWIR application with real thick lenses.



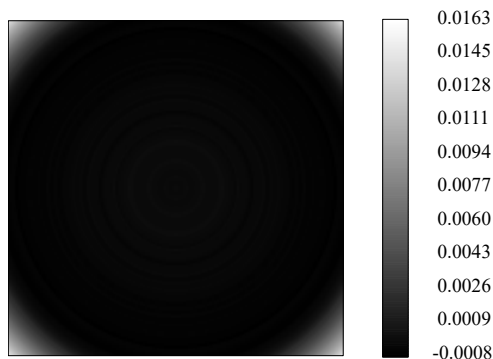
(a) Polychromatic Diffraction MTF.



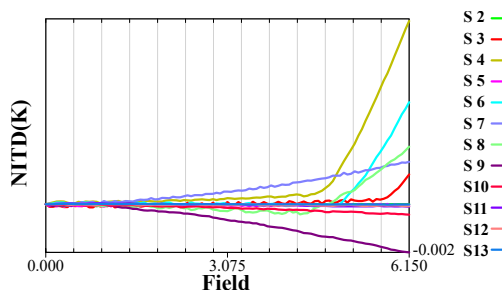
(b) RMS Spot Radius vs Field.



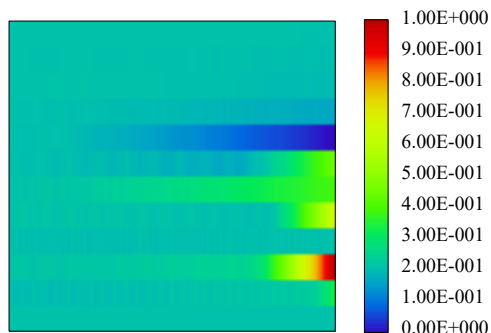
(c) Total NITD.



(d) 2D Narcissus Image.



(e) Surface Narcissus Contributions.



(f) 2D Surface Contributions.

Figure 4.8: Optical performance (a, b) and Narcissus performance (c, d, e f) of the LWIR application with real thick lenses.

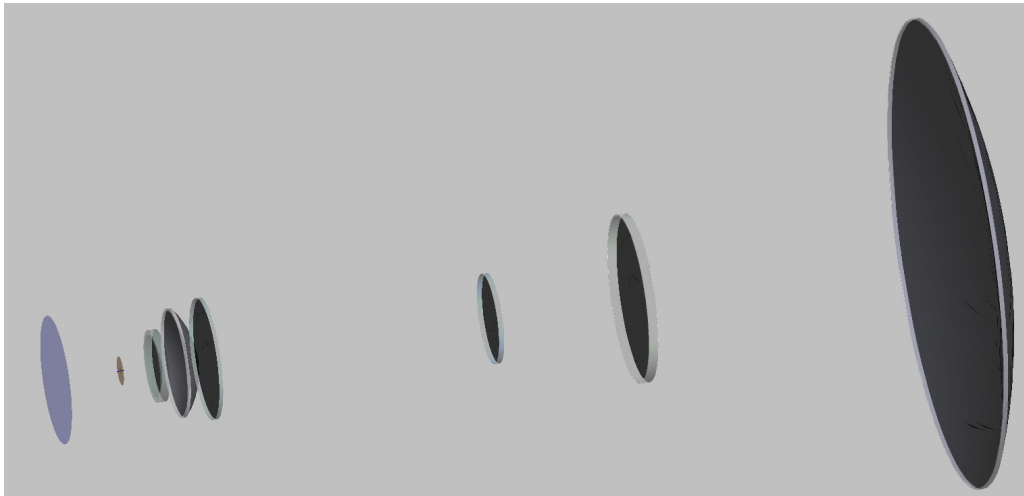
be analysed again. MTF and spot distribution of the infrared lens are given in Fig. 4.8. Optical performance does not change as expected and it is still close to the diffraction limited.

Narcissus performance must also be analysed after lens introduction to the lenses al-

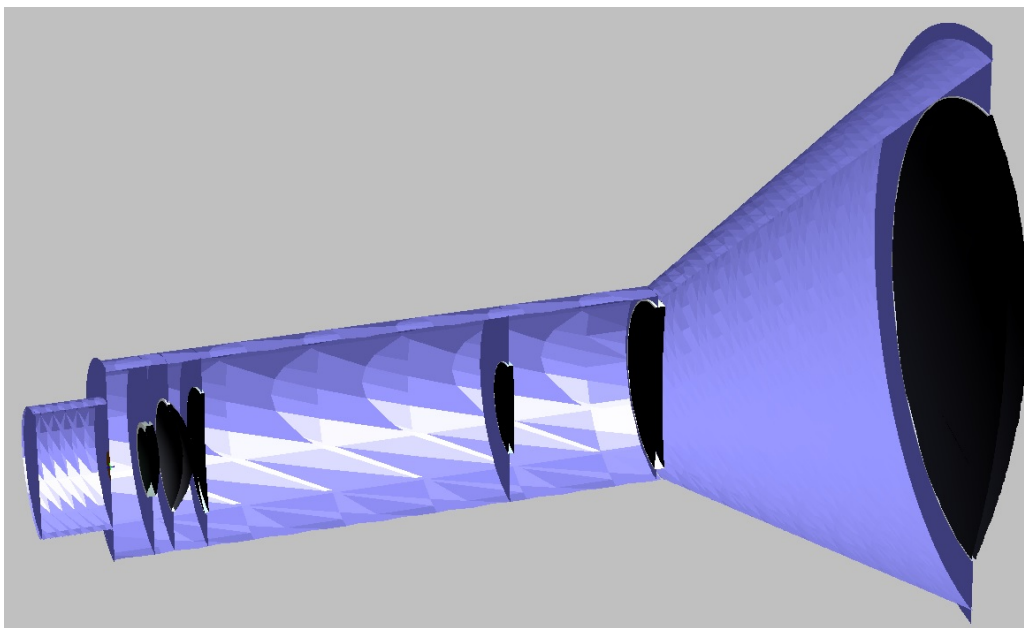
though very slight changes are observed in optical design after lenses are thickened. Results of real ray trace based analysis of narcissus at the detector plane are given in Fig. 4.8. Narcissus performance of the design is very similar to the design with zero thickness lenses. NITD level is 15-16 mK which is smaller than the noise equivalent level of the infrared detectors and image anomalies stemming from the narcissus effect will not be observed in infrared image.

In order to assess narcissus performance of LWIR lens non-sequentially with the help of thermal self emission analysis technique discussed in Chapter 2, a FRED model of LWIR lens is constructed. ZEMAX lens design is directly exported to FRED using built-in export tool in FRED environment. LWIR lens FRED model with and without opto-mechanical housing and detector dewar structure is shown in Fig. 4.9. In order to represent opto-mechanical housings and detector dewar structure, simple geometrical surfaces are used for the sake of ray-trace efficiency. Source properties, optical, opto-mechanical and detector surface properties are constructed according to the script described in Appendix B. Thermal self emission analysis results are shown in Fig. 4.10, 4.11, 4.12.

Both ZEMAX macro and FRED script give very close narcissus performance results for LWIR lens. Preparation of analysis model and carrying out narcissus analysis in ZEMAX is much faster, however, ZEMAX macro has many strict restrictions. Optical design to be analysed is assumed to have a rotational symmetry and radiation coming from opto-mechanical housing surfaces are assumed to be degraded uniformly and equally by the square of the transmission of the optics starting from the detector to the contributing narcissus surface. There is no symmetry assumption in FRED script and exact radiation from opto-mechanical surfaces are calculated non-sequentially, however, constructing the analysis model is complicated compared to ZEMAX and analysis time is much longer than ZEMAX macro. It is advisable to use ZEMAX macro in optical design phase of infrared lens. Once sufficient results are achieved in both imaging quality and narcissus perspective in ZEMAX, final narcissus performance must be checked with FRED script.



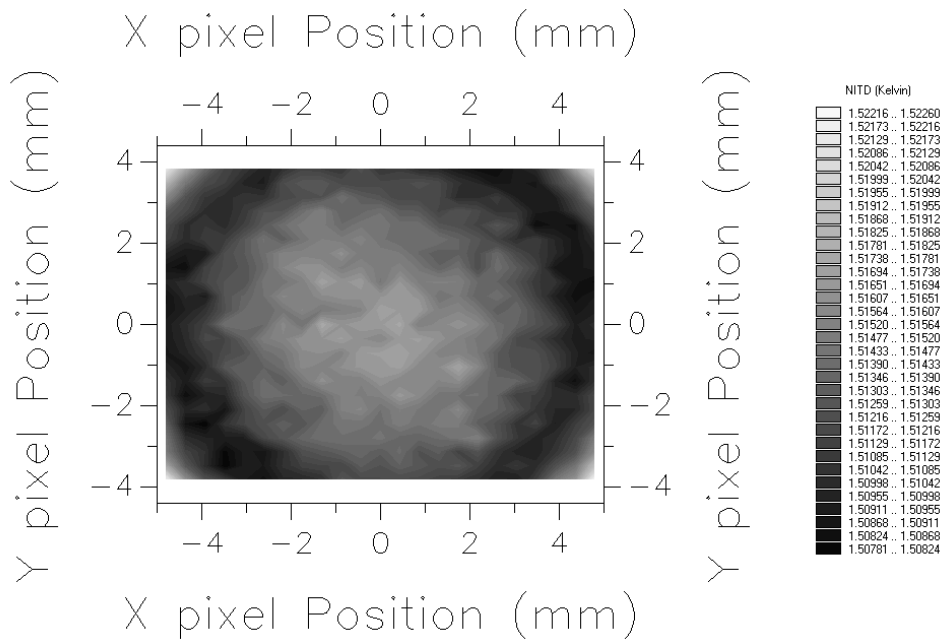
(a)



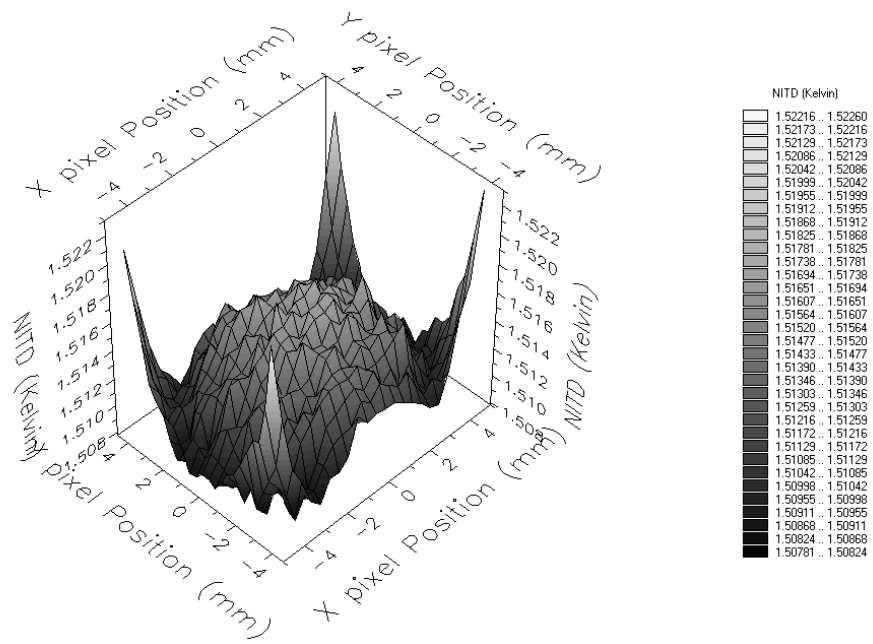
(b)

Figure 4.9: FRED models of LWIR application: (a) Model created by transporting ZEMAX design file to FRED, (b) Model where opto-mechanical surfaces and detector dewar structure are represented by simple geometrical surfaces.



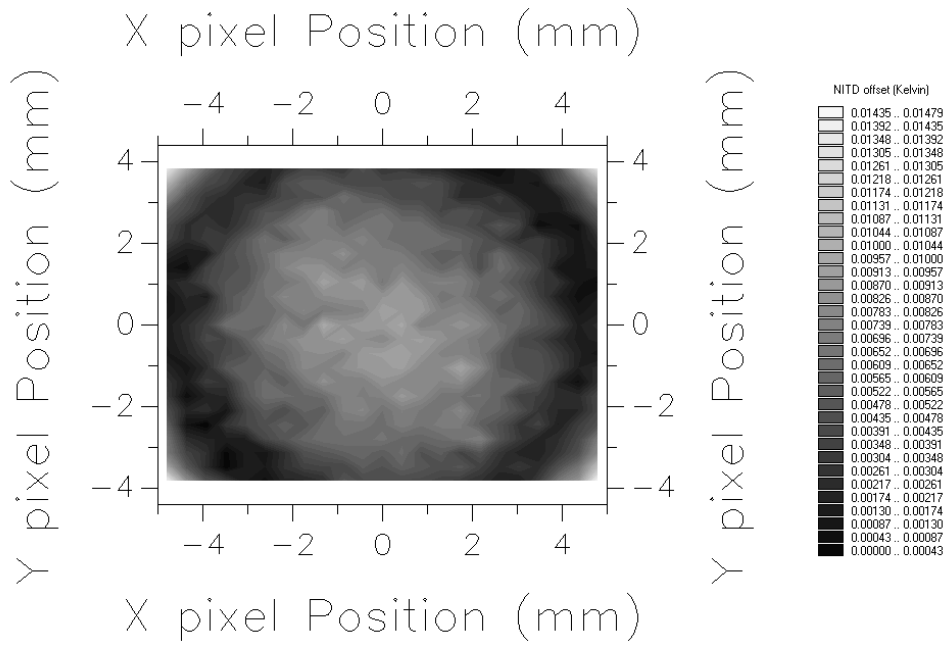


(a)

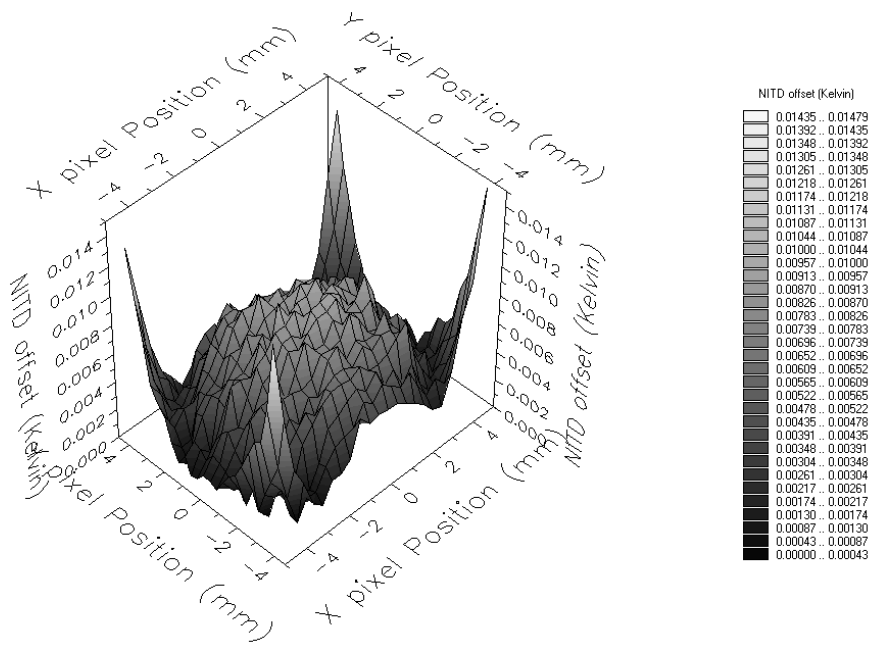


(b)

Figure 4.10: NITD performance of LWIR application analysed by script coded in FRED scripting environment: (a) NITD distribution, (b) NITD (perspective view).

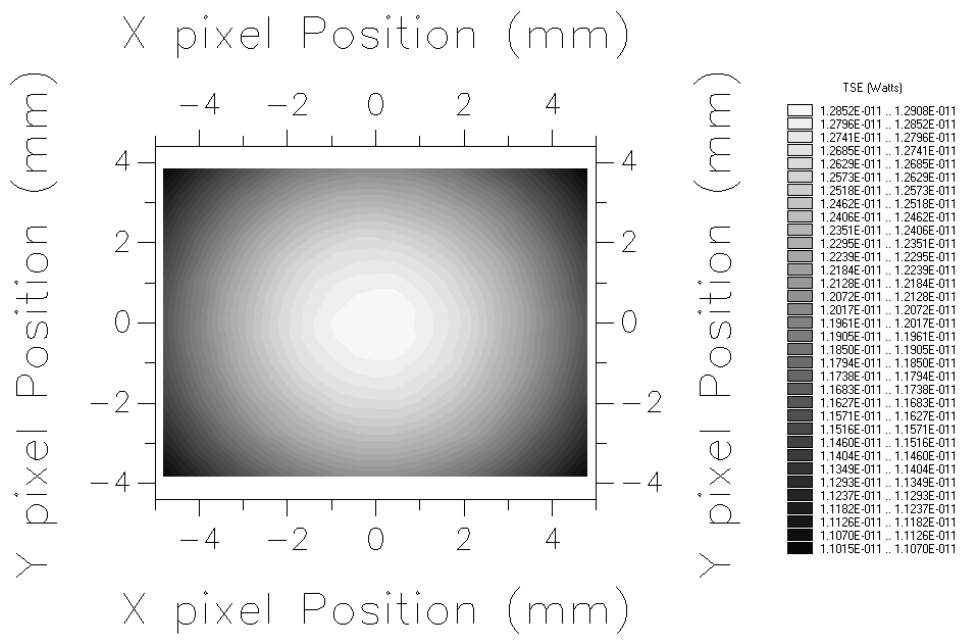


(a)

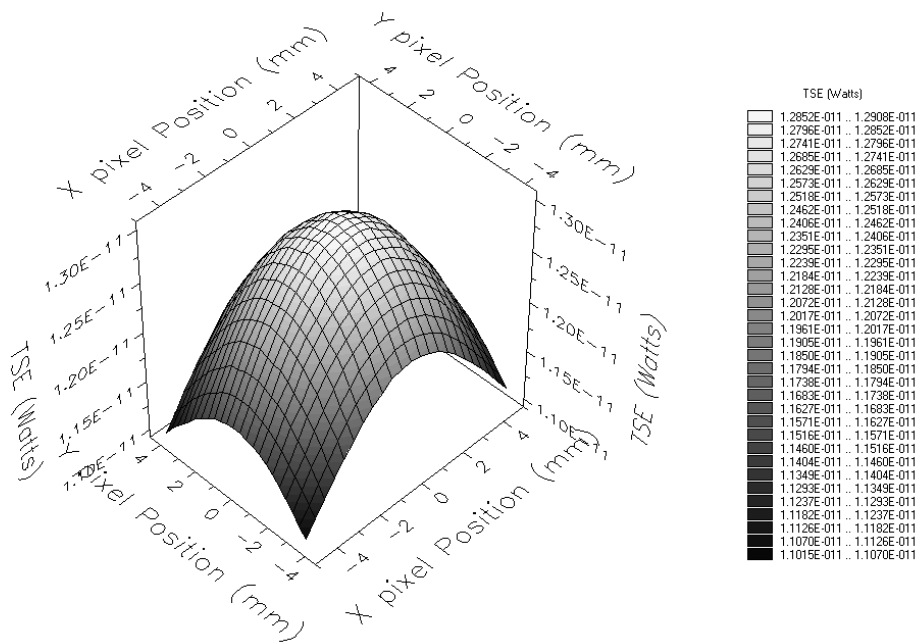


(b)

Figure 4.11: Offset NITD performance of LWIR application analysed by script coded in FRED scripting environment: (a) NITD offset corrected distribution, (b) NITD offset corrected (perspective view).



(a)



(b)

Figure 4.12: TSE distribution of LWIR application analysed by script coded in FRED scripting environment: (a) TSE distribution, (b) TSE (perspective view).



## CHAPTER 5

### CONCLUSION

In this thesis, narcissus effect in infrared lenses utilizing cooled infrared detectors is discussed in detail from optical design perspective. A narcissus model for paraxial lenses is proposed based on conventional narcissus controlling parameters which allows narcissus consideration in the early lens design stages and eliminates time consuming iterations between different starting points. Proposed narcissus model consists of two narcissus metrics which are expressed in terms of paraxial optical quantities of paraxial lenses in an optical design similar to the thin lens Seidel coefficients. Hence, proposed narcissus model combined with Seidel coefficients generates satisfactory starting points for infrared lens designs by enabling control on both optical aberrations and narcissus performance. A fictitious infrared lens operating in LWIR band is designed systematically including the proposed narcissus model as an application of the proposed narcissus model. Proposed narcissus model enables narcissus control in an indirect way. Therefore, a real raytrace based macro which calculates the final narcissus distribution or narcissus image at the detector plane is coded in ZPL platform. Using radiometric techniques and non-sequential ray-tracing capabilities of FRED, a script is also coded in FRED script environment in order to analyse narcissus effect. It is shown that LWIR lens designed with the proposed narcissus model has a satisfactory narcissus performance based on the NITD criterion which is proved to be smaller than the NETD of the infrared detector. As a consequence, image anomalies stemming from narcissus effect can not be discerned by the user since it is smaller than the sensitivity of the detector.

As a conclusion, a mathematical model of narcissus effect in infrared lenses with cooled detectors is constructed for a paraxial lens in terms of its paraxial optical

parameters in the paraxial form of an optical system for the first time and applied to a infrared lens design which operates in LWIR band systematically. It is shown that narcissus performance is controlled successfully in an indirect way, starting from the early paraxial design stage of the lens with the help of proposed narcissus model and final narcissus distribution at the detector plane is showed to be reduced below the infrared detector sensitivity level sufficiently by the narcissus macro coded in ZPL and the script coded in FRED.

## REFERENCES

- [1] H. Gross, F. Blechinger, and B. Achtner, *Handbook of Optical Systems, Volume 4: Survey of Optical Instruments*, ser. Gross/Optical Systems V1-V6 special prices until 6V ST published. Wiley, 2005.
- [2] J. Sasián, *Introduction to Aberrations in Optical Imaging Systems*. Cambridge University Press, 2012.
- [3] C. Velzel, *A Course in Lens Design*, ser. Springer Series in Optical Sciences. Springer Netherlands, 2014.
- [4] J. Vizgaitis and A. H. Jr., “Reducing narcissus with a GRIN,” in *Infrared Technology and Applications XLI*, B. F. Andresen, G. F. Fulop, C. M. Hanson, and P. R. Norton, Eds., vol. 9451, International Society for Optics and Photonics. SPIE, 2015, pp. 457 – 466. [Online]. Available: <https://doi.org/10.1117/12.2183589>
- [5] J. W. Howard and I. R. Abel, “Narcissus: reflections on retroreflections in thermal imaging systems,” *Appl. Opt.*, vol. 21, no. 18, pp. 3393–3397, Sep 1982. [Online]. Available: <http://opg.optica.org/ao/abstract.cfm?URI=ao-21-18-3393>
- [6] M. Riedl, *Optical Design Fundamentals for Infrared Systems*, ser. SPIE tutorial texts. Society of Photo Optical, 2001.
- [7] R. Kingslake and R. Johnson, *Lens Design Fundamentals*. Elsevier Science, 2009.
- [8] J. Bentley and C. Olson, *Field Guide to Lens Design*, ser. Field Guides. SPIE, 2012.
- [9] R. E. Fischer, “What’s so different about IR lens design?” in *Lens Design: A Critical Review*, W. J. Smith, Ed., vol. 10263, International Society for Optics and Photonics. SPIE, 1992, pp. 119 – 141. [Online]. Available: <https://doi.org/10.1117/12.131971>

- [10] “Opticstudio narcissus analysis macro,” accessed: 2021-03-31. [Online]. Available: <https://support.zemax.com/hc/en-us/articles/1500005487801-OpticStudio-narcissus-analysis-macro>
- [11] Ansys, “Zemax opticstudio,” Accessed: 02/04/2022. [Online]. Available: <https://www.zemax.com/pages/opticstudio>
- [12] J. Lloyd, *Thermal Imaging Systems*, ser. Optical physics and engineering. Plenum Press, 1975.
- [13] E. Dereniak and G. Boreman, *Infrared Detectors and Systems*, ser. Wiley Series in Pure and Applied Optics. Wiley, 1996.
- [14] “Sofradir galatea mwir surveillance,” accessed: 2022-03-26. [Online]. Available: <http://www.lynred.com/products/galatea-mw-surveillance>
- [15] A. S. Lau, “The Narcissus Effect In Infrared Optical Scanning Systems,” in *Stray Light Problems in Optical Systems*, J. D. Lytle and H. E. Morrow, Eds., vol. 0107, International Society for Optics and Photonics. SPIE, 1977, pp. 57 – 62. [Online]. Available: <https://doi.org/10.1117/12.964596>
- [16] E. H. Ford and D. M. Hasenauer, “Narcissus in current generation FLIR systems,” in *Infrared Optical Design and Fabrication: A Critical Review*, R. Hartmann and W. J. Smith, Eds., vol. 10260, International Society for Optics and Photonics. SPIE, 1991, pp. 77 – 101. [Online]. Available: <https://doi.org/10.1117/12.48446>
- [17] M. N. Akram, “Simulation and control of narcissus phenomenon using nonsequential ray tracing. i. staring camera in 3-5  $\mu\text{m}$  waveband,” *Appl. Opt.*, vol. 49, no. 6, pp. 964–975, Feb 2010. [Online]. Available: <http://opg.optica.org/ao/abstract.cfm?URI=ao-49-6-964>
- [18] R. N. Pfisterer, “Clever tricks in optical engineering,” in *Novel Optical Systems Design and Optimization VII*, J. M. Sasian, R. J. Koschel, P. K. Manhart, and R. C. Juergens, Eds., vol. 5524, International Society for Optics and Photonics. SPIE, 2004, pp. 230 – 239. [Online]. Available: <https://doi.org/10.1117/12.566399>



- [19] P. Engineering, “Fred,” Accessed: 02/04/2022. [Online]. Available: <https://photonengr.com/fred-software/>
- [20] H. Hopkins, *Wave Theory of Aberrations*, ser. Monographs on the physics and chemistry of materials. Clarendon Press, 1950.
- [21] K. Thompson, “Description of the third-order optical aberrations of near-circular pupil optical systems without symmetry,” *J. Opt. Soc. Am. A*, vol. 22, no. 7, pp. 1389–1401, Jul 2005. [Online]. Available: <http://opg.optica.org/josaa/abstract.cfm?URI=josaa-22-7-1389>
- [22] H. Gross, H. Zügge, M. Peschka, and F. Blechinger, *Handbook of Optical Systems, Volume 3: Aberration Theory and Correction of Optical Systems*, ser. Gross/Optical Systems V1-V6 special prices until 6V ST published (VCH). Wiley, 2007.
- [23] J. L. Bentley, C. Olson, and R. N. Youngworth, “In the era of global optimization, the understanding of aberrations remains the key to designing superior optical systems,” in *Optical Design and Testing IV*, Y. Wang, J. Bentley, C. Du, K. Tatsuno, and H. P. Urbach, Eds., vol. 7849, International Society for Optics and Photonics. SPIE, 2010, pp. 101 – 113. [Online]. Available: <https://doi.org/10.1117/12.871720>
- [24] M. J. Kidger, “Importance of aberration theory in understanding lens design,” in *Fifth International Topical Meeting on Education and Training in Optics*, C. H. F. Velzel, Ed., vol. 3190, International Society for Optics and Photonics. SPIE, 1997, pp. 26 – 33. [Online]. Available: <https://doi.org/10.1117/12.294396>
- [25] S. H. Aslan and S. K. Yerli, “Thin lens narcissus model in infrared lens design with cooled detectors,” *Appl. Opt.*, vol. 61, no. 3, pp. 728–736, Jan 2022. [Online]. Available: <http://opg.optica.org/ao/abstract.cfm?URI=ao-61-3-728>
- [26] J. L. Rayces and L. Lebach, “Exact ray-tracing computation of narcissus-equivalent temperature difference in scanning thermal imagers,” in *Current Developments in Optical Design and Optical Engineering II*, R. E. Fischer and W. J. Smith, Eds., vol. 1752, International Society for

Optics and Photonics. SPIE, 1992, pp. 325 – 332. [Online]. Available: <https://doi.org/10.1117/12.130755>

- [27] K. Lu and S. J. Dobson, “Accurate calculation of narcissus signatures by using finite ray tracing,” *Appl. Opt.*, vol. 36, no. 25, pp. 6393–6398, Sep 1997. [Online]. Available: <http://ao.osa.org/abstract.cfm?URI=ao-36-25-6393>
- [28] Y. Reibel, A. Rouvie, A. Nedelcu, T. Augey, N. Pere-Laperne, L. Rubaldo, D. Billon-Lanfrey, O. Gravrand, J. Rothman, and G. Destefanis, “Large format, small pixel pitch and hot detectors at SOFRADIR,” in *Electro-Optical and Infrared Systems: Technology and Applications X*, D. A. Huckridge and R. Ebert, Eds., vol. 8896, International Society for Optics and Photonics. SPIE, 2013, pp. 70 – 80. [Online]. Available: <https://doi.org/10.1117/12.2030698>
- [29] S. Hanna, D. Eich, W. Fick, H. Figgemeier, M. Mahlein, W. Schirmacher, and R. Thöt, “Low dark current LWIR and VLWIR HgCdTe focal plane arrays at AIM,” in *Sensors, Systems, and Next-Generation Satellites XX*, R. Meynart, S. P. Neeck, and T. Kimura, Eds., vol. 10000, International Society for Optics and Photonics. SPIE, 2016, pp. 135 – 153. [Online]. Available: <https://doi.org/10.1117/12.2244514>

## APPENDIX A

### ZEMAX NARCISSUS MACRO

```
!Narcissus Analysis
!
!This macro calculates narcissus induced temperature difference (Nitd)
!in infrared designs with cooled detectors.
!
!Restrictions and Assumptions:
!
!1)Lens must be designed from detector to ambient.
!2)Cold stop surface must be surface 1.
!3)Design must not have any coordinate breaks or dummy surfaces.
!4)Design must be rotationally symmetric.
!5)Only single configuration designs are supported.
!6)Single bounce ghost files must be generated starting from surface 2
!with Zemax Ghost Focus Generator tool, and saved into the design file
!folder before running the macro.
!7-)Normalized detector spectral response is assumed to be constant over
!operating wavelengths, so this parameter is not needed in calculations.
!8-)Atmospheric transmittance is assumed to be 1 which means that NITD
!is referenced to the ambient temperature just in front of the lens.
!9-)Performance of all coatings applied on lens surfaces is assumed to
!be constant over operating wavelengths.
!10-)Housing and detector are assumed to be at constant temperature which
!means that there is no temperature gradient in instrument housing and
!detector.

!User inputs:
!1) Single bounce ghost files in design file folder
!2) Housing temperature
!3) Detector temperature
!4) Ambient temperature
!5) Ray density and Field density for vignetting plot( "Save" must be
!clicked after density values are entered).
!
!outputs:
!
!Graph 1) Surface NITD Contributions vs Field (off-axis reference)
!Graph 2) Surface NITD Contributions vs Field (on-axis reference)
!Graph 3) 3D NITD Surface Contributions (Surface plot)
!Graph 4) False colour 2D NITD Surface Contributions (Range of scale is
defined as default(0 to 1))
!Graph 5) Total NITD vs Field (on-axis and off-axis reference)
!Graph 6) Inverse Greyscale 2D Total NITD across FPA in Kelvin scale
!(diagonal FPA size is shown)
!Textfile: Design file name, Operating wavelength, Temperature data,
!Number of ghost files, Optical transmission, Nitd surface contributions,
```

```

!Total Nitd(off-axis), Total Nitd(on-axis),
!Surface cold return vignetting data, Ghost files transmission
!data, Surface Yni data, Surface i/ibar data
!
!
!Author : Serhat Hasan ASLAN
!Company: ASELSAN - MGEO
!Contact: shaslan@aselsan.com.tr
!
!

!!!!!!!!!!!!!!!!!!!!!!!!!!!!Check stop position and dummy surfaces!!!!!!!!!!!!!!!!!!!!

setvecsize 10000
getsystemdata 1

if (vec1(23) != 1)
    print "stop surface must be surface 1"
end
else
endif

for i,1,nsur()-2,1

    format 2.10

    dummy = spro(i,4)
    glass_name$ = $buffer()
    glass_number = spro(i,18)

    dummy = spro(i+1,4)
    glass_name2$ = $buffer()
    glass_number2 = spro(i+1,18)

if ((glass_number == 0) & (glass_name$ $!= "MIRROR"))

if ((glass_number2 == 0)&(glass_name2$ $!= "MIRROR"))
print " Error: Dummy surface detected." + $STR(i+1)
end
else
endif
else
endif

if (glass_name$ $== "MIRROR")

if ((glass_number2 == 0)&(glass_name2$ $!= "MIRROR"))
print " Error: Dummy surface detected." + $STR(i+1)
end
else
endif
else
endif

next

!!!!!!!!!!!!!!!!!!!!!!!!!!!!count the number of ghost files!!!!!!!!!!!!!!!!!!!!!!!!!!!!

file_dir$ = $filepath()
path$ = $pathname()

```

```

prefix$ = "\GH0"

! Test for ZMX files first
FILTER$ = path$ + prefix$ + "*.ZMX"
PRINT "Listing of all Zemax files in ", FILTER$
FINDFILE TEMPFILE$, FILTER$
numZMXFiles = 0
numZOSFiles = 0
NumOfGhostFiles = 0

LABEL 1
IF (SLEN(TEMPFILE$))
FINDFILE TEMPFILE$, FILTER$
numZMXFiles = numZMXFiles + 1
GOTO 1
ENDIF

IF numZMXFiles == 0
FILTER$ = path$ + prefix$ + "*.ZOS"
FINDFILE TEMPFILE$, FILTER$
LABEL 2
IF (SLEN(TEMPFILE$))
FINDFILE TEMPFILE$, FILTER$
numZOSFiles = numZOSFiles + 1
GOTO 2
ENDIF
ENDIF

FORMAT 3.0

IF numZMXFiles > 0
NumOfGhostFiles = numZMXFiles
ext$ = ".zmx"
ENDIF
IF numZOSFiles > 0
NumOfGhostFiles = numZOSFiles
ext$ = ".zos"
ENDIF
IF (numZMXFiles == 0) & (numZOSFiles == 0)
PRINT "Error: Ghostfiles are not generated"
END
ENDIF

!!!!!!!!!!!!!!check coatings!!!!!!!!!!!!!!

for i,2,NumOfGhostFiles+1,1

dummy = SPRO(i,8)
a$ = $buffer()
b$ = "0"
c$ = b$ + $rightstring(a$,3)
format 5.5
coat_perf = SVAL(c$)

format 3.0
if coat_perf == 0
message$ = "Warning: Coating is not assigned to surface " + $STR(i)
print message$
else
endif

```

```

format 5.5

next

!!!!!!!!!!!!!!!!!!!!!!!!!!!!!!!!!!!!!!!!!!!!!!!!!!!!!!!!!!!!!!!!!!!!!!!!!!!!!!!!!!!!!!!!!!!!!!!!!!!!!!!!!!!!!!!!!!!!!!!!

input "Enter Housing Temperature in Kelvin:", h_temp

if (h_temp<200) | (h_temp>400)
print " Error: Invalid housing temperature."
end
else
endif

input "Enter Detector Temperature in Kelvin:", d_temp

if (d_temp<0) | (d_temp>200)
print " Error: Invalid detector temperature."
end
else
endif

input "Enter Ambiance Temperature in Kelvin:", a_temp

if (a_temp<200) | (a_temp>400)
print " Error: Invalid ambiance temperature."
end
else
endif

!!!!!!generate field vector,vignetting vector,transmission vector!!!!!!

poltrace 0,0,0,0,pwav(),4,nsur()
opt_trans = vec4(1)

vig_data$ = path$ + "\vignetting_set.txt"
gettextfile vig_data$, Vig, "vig_set.cfg ",2

open vig_data$

for j,1,12,1
readstring x
next

field_sample = 0

label count
readstring A$
field_sample = field_sample + 1

if (!eof()) then goto count
field_sample = field_sample - 1

close vig_data$
deletefile vig_data$

for i,2,NumOfGhostFiles+1,1

format "%#05i" LIT

```



```

x_par_wavl_d = h*c/(VECl(field_sample+1)*expt(-6))/k/d_temp
x_par_wavf_d = h*c/(VECl(field_sample+nwav())*expt(-6))/k/d_temp

if (VECl(field_sample+nwav())*h_temp < 2500)

fe_will_h_w1 = 90/powr(pi,4)*expe(-x_par_wavl_h ) *
(1+x_par_wavl_h + powr(x_par_wavl_h,2)/2 + powr(x_par_wavl_h,3)/6) *
(1+(VECl(field_sample+1)*h_temp-2500)/150000)
fe_will_h_wf = 90/powr(pi,4)*expe(-x_par_wavf_h ) *
(1+x_par_wavf_h + powr(x_par_wavf_h,2)/2 + powr(x_par_wavf_h,3)/6) *
(1+(VECl(field_sample+nwav())*h_temp-2500)/150000)
fe_will_d_w1 = 90/powr(pi,4)*expe(-x_par_wavl_d ) *
(1+x_par_wavl_d + powr(x_par_wavl_d,2)/2 + powr(x_par_wavl_d,3)/6) *
(1+(VECl(field_sample+1)*d_temp-2500)/150000)
fe_will_d_wf = 90/powr(pi,4)*expe(-x_par_wavf_d ) *
(1+x_par_wavf_d + powr(x_par_wavf_d,2)/2 + powr(x_par_wavf_d,3)/6) *
(1+(VECl(field_sample+nwav())*d_temp-2500)/150000)

else

fe_will_h_w1 = 90/powr(pi,4)*expe(-x_par_wavl_h ) *
(1+x_par_wavl_h + powr(x_par_wavl_h,2)/2 + powr(x_par_wavl_h,3)/6)
fe_will_h_wf = 90/powr(pi,4)*expe(-x_par_wavf_h ) *
(1+x_par_wavf_h + powr(x_par_wavf_h,2)/2 + powr(x_par_wavf_h,3)/6)
fe_will_d_w1 = 90/powr(pi,4)*expe(-x_par_wavl_d ) *
(1+x_par_wavl_d + powr(x_par_wavl_d,2)/2 + powr(x_par_wavl_d,3)/6)
fe_will_d_wf = 90/powr(pi,4)*expe(-x_par_wavf_d ) *
(1+x_par_wavf_d + powr(x_par_wavf_d,2)/2 + powr(x_par_wavf_d,3)/6)

endif

narc_coef_1 = tot_integ_h * (fe_will_h_wf - fe_will_h_w1 )/pi -
tot_integ_d * (fe_will_d_wf - fe_will_d_w1 )/pi

tot_integ_a = sigma * powr(a_temp,4)
tot_integ_a_delta = sigma * powr((a_temp+0.001),4)

x_par_wavl_a = h*c/(VECl(field_sample+1)*expt(-6))/k/a_temp
x_par_wavf_a = h*c/(VECl(field_sample+nwav())*expt(-6))/k/a_temp
x_par_wavl_a_delta = h*c/(VECl(field_sample+1)*expt(-6))/k/(a_temp+0.001)
x_par_wavf_a_delta = h*c/(VECl(field_sample+nwav())*expt(-6))/k/(a_temp+0.001)

if (VECl(field_sample+nwav())*a_temp < 2500)

fe_will_a_w1 = 90/powr(pi,4)*expe(-x_par_wavl_a )*(1+x_par_wavl_a +
powr(x_par_wavl_a,2)/2 + powr(x_par_wavl_a,3)/6) *
(1+(VECl(field_sample+1)*a_temp-2500)/150000)
fe_will_a_wf = 90/powr(pi,4)*expe(-x_par_wavf_a )*(1+x_par_wavf_a +
powr(x_par_wavf_a,2)/2 + powr(x_par_wavf_a,3)/6) *
(1+(VECl(field_sample+nwav())*a_temp-2500)/150000)
fe_will_a_delta_w1 = 90/powr(pi,4)*expe(-x_par_wavl_a_delta ) *
(1+x_par_wavl_a_delta + powr(x_par_wavl_a_delta,2)/2 +
powr(x_par_wavl_a_delta,3)/6) * (1+(VECl(field_sample+1)*
(a_temp+0.001)-2500)/150000)
fe_will_a_delta_wf = 90/powr(pi,4)*expe(-x_par_wavf_a_delta ) *
(1+x_par_wavf_a_delta + powr(x_par_wavf_a_delta,2)/2 +
powr(x_par_wavf_a_delta,3)/6) * (1+(VECl(field_sample+nwav())*
(a_temp+0.001)-2500)/150000)

else

```



```

fe_will_a_w1 = 90/powr(pi,4)*expe(-x_par_wav1_a ) *
(1+x_par_wav1_a + powr(x_par_wav1_a,2)/2 + powr(x_par_wav1_a,3)/6)
fe_will_a_wf = 90/powr(pi,4)*expe(-x_par_wavf_a ) *
(1+x_par_wavf_a + powr(x_par_wavf_a,2)/2 + powr(x_par_wavf_a,3)/6)
fe_will_a_delta_w1 = 90/powr(pi,4)*expe(-x_par_wav1_a_delta ) *
(1+x_par_wav1_a_delta + powr(x_par_wav1_a_delta,2)/2 +
powr(x_par_wav1_a_delta,3)/6)
fe_will_a_delta_wf = 90/powr(pi,4)*expe(-x_par_wavf_a_delta ) *
(1+x_par_wavf_a_delta + powr(x_par_wavf_a_delta,2)/2 +
powr(x_par_wavf_a_delta,3)/6)

endif

narc_coef_2 = (tot_integ_a_delta * (fe_will_a_delta_wf -
fe_will_a_delta_w1 )/pi - tot_integ_a *
(fe_will_a_wf - fe_will_a_w1 )/pi)/0.001

narc_coefficient = narc_coef_1/narc_coef_2

!!calc NITD vector

for m,2,NumOfGhostFiles+1,1

for n,1,field_sample,1

nitd = VEC2(field_sample*(m-2)+n) * narc_coefficient * VEC3(m-1)
VEC4 field_sample*(m-2)+n, nitd

next

next

max_nitd_surf = VEC4(1)

!!calc maximum of NITD vector

for i,1,field_sample*NumOfGhostFiles,1
if (VEC4(i) > max_nitd_surf)
max_nitd_surf = VEC4(i)
else
endif
next

!!!!calc total surface NITD contributions vector

nitd_field = 0

for i,1,field_sample,1
for j,2,NumOfGhostFiles+1,1
nitd_field = nitd_field + vEC4(field_sample*(j-2) + i)
next
VEC4(field_sample*NumOfGhostFiles+i) = nitd_field
nitd_field = 0

next

!!calc maximum and minimum of total NITD vector

max_nitd = -10000

```

```

min_nitd = 10000

for i, (field_sample*(NumOfGhostFiles)+1), (field_sample*(NumOfGhostFiles+1)), 1
if (VEC4(i) > max_nitd)
max_nitd = VEC4(i)
else
endif

if (VEC4(i) < min_nitd)
min_nitd = VEC4(i)
else
endif

next

!!!!!!!!!!!!!!!!!!!!!!!!!!!!Plot!!!!!!!!!!!!!!!!!!!!!!!!!!!!!!!!!!!!

!! plot NITD Surface contributions (off-axis reference)

declare nitd_surf, double, 1, field_sample
declare nitd_surf2, double, 1, field_sample
declare nitd_total_offAxis, double, 1, field_sample
declare nitd_total_onAxis, double, 1, field_sample
declare field, double, 1, field_sample
declare label_array_x, double, 1, 2
declare label_array_y, double, 1, 2

int_part = inte(field_sample/NumofGhostFiles)
2Darray_ysize = int_part * NumofGhostFiles
declare nitd_surf_2Darray, double, 2 , field_sample, 2Darray_ysize

format 5.3
plot new
plot title, "          Surface NITD Contributions (off-axis reference)"
plot banner, "Narcissus Analysis"
plot titlex, "Field"
plot titley, "NITD(K) "
plot rangex, 0 , vec1(field_sample)
plot rangey, 0 , max_nitd_surf + 0.0001
plot tick, VEC1(field_sample)/13, (max_nitd_surf + 0.0001)/10

h$ = "Housing temperature in Kelvin = " + $STR(h_temp)
a$ = "Ambiance temperature in Kelvin = " + $STR(a_temp)
d$ = "Detector temperature in Kelvin = " + $STR(d_temp)
plot comm1, h$
plot comm2, a$
plot comm3, d$
plot comm4, ""
plot comm5, ""
plot comm6, ""

for i, 2, NumOfGhostFiles+1, 1

for j, 1, field_sample, 1
nitd_surf(j) = VEC4(field_sample*(i-2)+j)
field(j) = VEC1(j)
next

plot data, field, nitd_surf, field_sample, i, 0

```

```

label_array_x(1) = vec1(field_sample)*(1+0.20)
label_array_x(2) = vec1(field_sample)*(1+0.25)
label_array_y(1) = (max_nitd_surf / (NumOfGhostFiles-1)) *
(NumOfGhostFiles-(i-1))
label_array_y(2) = (max_nitd_surf / (NumOfGhostFiles-1)) *
(NumOfGhostFiles-(i-1))

plot data, label_array_x, label_array_y, 2, i, 0

format 2.0
surface$ = "S" + $STR(i)
plot label, 0.91, 0.295+(NumOfGhostFiles-(i-1))/(NumOfGhostFiles-1)*
0.6,0, 0.7,surface$

next

plot go

!! plot NITD Surface contributions (on-axis reference)

format 5.3

max_nitd_surf2 = 0
min_nitd_surf2 = 10000

for i,2,NumOfGhostFiles+1,1

for j,1,field_sample,1
nitd_surf2(j) = VEC4(field_sample*(i-2)+1)-VEC4(field_sample*(i-2)+j)
if(nitd_surf2(j) < min_nitd_surf2)
min_nitd_surf2 = nitd_surf2(j)
else
endif

if(nitd_surf2(j) > max_nitd_surf2)
max_nitd_surf2 = nitd_surf2(j)
else
endif

field(j) = VEC1(j)
next
next

plot new
plot title, "          Surface NITD Contributions (on-axis reference)"
plot banner,"Narcissus Analysis"
plot titlex, "Field"
plot titley, "NITD(K) "
plot rangex, 0 , vec1(field_sample)
plot rangey, min_nitd_surf2 , max_nitd_surf2 + 0.0001
plot tick,VEC1(field_sample)/13, (max_nitd_surf + 0.0001)/10

plot comm1,h$
plot comm2,a$
plot comm3,d$
plot comm4,""
plot comm5,""
plot comm6,""

for i,2,NumOfGhostFiles+1,1

```

```

for k,1,int_part,1
for j,1,field_sample,1
nitd_surf2(j) = VEC4(field_sample*(i-2)+1)-VEC4(field_sample*(i-2)+j)
field(j) = VEC1(j)
y_index = int_part*(i-2)+k
nitd_surf_2Darray(j,y_index) = nitd_surf2(j)
next
next

plot data, field, nitd_surf2, field_sample, i, 0

label_array_x(1) = vec1(field_sample)*(1+0.20)
label_array_x(2) = vec1(field_sample)*(1+0.25)
label_array_y(1) = ((max_nitd_surf2-min_nitd_surf2)/ (NumOfGhostFiles-1)) *
(NumOfGhostFiles-(i-1)) + min_nitd_surf2
label_array_y(2) = ((max_nitd_surf2-min_nitd_surf2)/ (NumOfGhostFiles-1)) *
(NumOfGhostFiles-(i-1)) + min_nitd_surf2

plot data, label_array_x, label_array_y, 2, i, 0

format 2.0
surface$ = "S" + $STR(i)
plot label, 0.91, 0.295+(NumOfGhostFiles-(i-1))/(NumOfGhostFiles-1)*
0.6,0, 0.7,surface$
format 5.3
next

plot go

plot2d new
plot2d title, "Narcissus Analysis: Surface NITD Contributions"
plot2d data, nitd_surf_2Darray
plot2d displaytype,1
plot2d comm1,h$
plot2d comm2,a$
plot2d comm3,d$
format 2.0
comm$ = "Surface number increases upwards from S2 to S" +
$STR(NumOfGhostFiles+1)
plot2d comm4,comm$
plot2d comm5,""
plot2d comm6,""
plot2d go

plot2d new
plot2d title, "Narcissus Analysis: Surface NITD Contributions"
plot2d data, nitd_surf_2Darray
plot2d displaytype,5
plot2d comm1,h$
plot2d comm2,a$
plot2d comm3,d$
plot2d comm4,comm$
plot2d comm5,""
plot2d comm6,""
plot2d go

!! plot total NITD(off-axis and on-axis reference)

format 5.3
max_nitd_off = -1000

```

```

min_nitd_off = 1000
max_nitd_on = -1000
min_nitd_on = 1000

for i,1,field_sample,1

nitd_total_offAxis(i) = (VEC4(field_sample*NumOfGhostFiles+i) - min_nitd)

if (nitd_total_offAxis(i)<min_nitd_off)
min_nitd_off = nitd_total_offAxis(i)
else
endif
if (nitd_total_offAxis(i)>max_nitd_off)
max_nitd_off = nitd_total_offAxis(i)
else
endif

nitd_total_onAxis(i) = nitd_total_offAxis(1) - nitd_total_offAxis(i)

if (nitd_total_onAxis(i)<min_nitd_on)
min_nitd_on = nitd_total_onAxis(i)
else
endif
if (nitd_total_onAxis(i)>max_nitd_on)
max_nitd_on = nitd_total_onAxis(i)
else
endif
field(i) = VEC1(i)

next

if (min_nitd_on < min_nitd_off)
min_nitd = min_nitd_on
else
min_nitd = min_nitd_off
endif

if (max_nitd_on > max_nitd_off)
max_nitd = max_nitd_on
else
max_nitd = max_nitd_off
endif

plot new
plot title, "Total NITD"
plot banner,"Narcissus Analysis"
plot titlex, "Field"
plot titley, "NITD(K)"
plot rangex, 0 , vec1(field_sample)
plot rangey, min_nitd , max_nitd
plot tick,VEC1(field_sample)/13, (max_nitd - min_nitd)/10

plot data, field, nitd_total_offAxis, field_sample, 1, 0
plot data, field, nitd_total_onAxis, field_sample, 2, 0

for i,1,2,1

label_array_x(1) = vec1(field_sample)*(1+0.20)
label_array_x(2) = vec1(field_sample)*(1+0.25)

```

```

label_array_y(1) = (max_nitd - min_nitd)*i/3 + min_nitd
label_array_y(2) = (max_nitd - min_nitd)*i/3 + min_nitd

plot data, label_array_x, label_array_y, 2, i, 0

format 2.0
if (i==1)
plot label, 0.91, 0.45,0, 0.7,"offAxis Ref"
else
plot label, 0.91, 0.65,0, 0.7,"onAxis Ref"
endif
next

plot go

!!plot2d NITD(on-axis reference)

nitd_array_size = inte(field_sample/powr(2,0.5))
nitd_array_quad_size = 2*nitd_array_size-1
declare nitd_array_quad,double,2,nitd_array_quad_size,
nitd_array_quad_size

for i,1,nitd_array_quad_size ,1
for j,1,nitd_array_quad_size ,1
delta_r = powr((powr( (i-nitd_array_size),2)+
powr((j-nitd_array_size),2)),0.5)

if(delta_r == 0)
delta_r = 1
else
endif

nitd_array_quad(i,j) = (nitd_total_onAxis(inte(delta_r)+1) -
nitd_total_onAxis(inte(delta_r)))*(delta_r-inte(delta_r)) +
nitd_total_onAxis(inte(delta_r))

next
next

format 5.5

plot2d new
plot2d title, "Narcissus Analysis: NITD distribution over FPA"
plot2d range, min_nitd_on, max_nitd_on
plot2d data, nitd_array_quad
plot2d displaytype,4
plot2d comm1,h$
plot2d comm2,a$
plot2d comm3,d$
plot2d comm4,""
plot2d comm5,""
plot2d comm6,""
plot2d go

!!!!!!!!!!!!!!!!!!!!!!!!!!!!!!!!!!!!!!!!!!!!!!!!!!!!!!!!!!!!!!!!!!!!!!!!!!!!

path$ = $pathname()
prefix$ = "\NarcAnalysis Results.txt"
results_data_file$ = path$ + prefix$
output results_data_file$

```

```

print "Narcissus Analysis"
print ""
print "File: ", file_dir$
print "Date: ", $date()
print ""

format 2.4
print "Operating wavelength: ",VEC1(field_sample+1)," to ",
VEC1(field_sample+nwav())," um."
print "Housing temperature in Kelvin: ", h_temp
print "Ambiance temperature in Kelvin: ", a_temp
print "Detector temperature in Kelvin: ", d_temp
format 3.0
print "Number of cold return surfaces: ", NumOfGhostFiles
format 2.4
print "optical transmission: ", opt_trans

print ""

!!!!!!!print nitd data

print ""
print "Nitd Data"
print ""

format 2.0
header$ = ""
for i,2,NumOfGhostFiles+1,1

header$ = header$ + "Surface " + $STR(i) + "      "

next

header$ = "Field          " + header$ + " NITD(off-axis ref.) " +
" NITD(on-axis ref.) "
print header$

format 3.6
for i,1,field_sample,1
header$ = $STR(VEC1(i))

for j,2,NumOfGhostFiles+1,1
header$ = header$ + "          " + $STR(VEC4(field_sample*(j-2)+i))
next

header$ = header$ + "          " + $STR(nitd_total_offAxis(i)) +
"          " + $STR(nitd_total_onAxis(i))
print header$
next

!!!!!!!print cold return vignetting data

print ""
print ""
print "Cold Return Vignetting Data"
print ""

format 2.0

```

```

header$ = ""

for i,2,NumOfGhostFiles+1,1

header$ = header$ + "Surface " + $STR(i) + "      "

next

header$ = "Field          " + header$
print header$

format 3.6
for i,1,field_sample,1

header$ = $STR(VEC1(i))

for j,2,NumOfGhostFiles+1,1
header$ = header$ + "          " + $STR(VEC2(field_sample*(j-2)+i))
next

print header$
next

print ""
print ""
print "Transmission Data"
print ""

header$ = "Surface          " + "Transmission "
print header$

for j,2,NumOfGhostFiles+1,1
format 4.0
header$ = $STR(j)
format 3.6
header$ = header$ + "          " + $STR(VEC3(j-1)*opt_trans)
print header$
next

!!!!!!!print yni data

print ""
print ""
print "Yni Data"
print ""
yni_data$ = path$ + "\yni.txt"
gettextfile yni_data$, Yni

open yni_data$

for j,1,10,1
readstring x
next

label count2
readstring A$
print A$

```



```

if (!eof()) then goto count2

close yni_data$
deletefile yni_data$

!!!!!!!print i/ibar data

declare i_ibar, double, 1,NumOfGhostFiles+1

for i,2,NumOfGhostFiles+1,1

raid_code = ocod("RAID")
ang_onaxis = opev(raid_code ,i,2,0,0,0,1)
ang_offaxis = opev(raid_code ,i,2,0,1,0,0)
i_ibar(i) = ang_onaxis / ang_offaxis

next

print ""
print ""
print "i/ibar Data"
print ""

header$ = "Surface      " + "i/ibar"
print header$

for j,2,NumOfGhostFiles+1,1
format 4.0
header$ = $STR(j)
format 3.6
header$ = header$ +"      " + $STR(i_ibar(j))
print header$
next

!!!!!!!Analysis End

output screen

print "Narcissus Analysis completed.
'NarcAnalysisResults.txt' file is created."

```



## APPENDIX B

### FRED NARCISSUS SCRIPT

```
'Narcissus Analysis
,
'This macro calculates narcissus induced temperature difference (NITD) in
infrared designs with cooled detectors in FRED platform.
,
'Restrictions and Assumptions:
,
'1-) Atmospheric transmittance is assumed to be 1 which means that NITD is
referenced to the ambient temperature just in front of the lens.
'2-) Housing and detector are assumed to be at constant temperature which
means that there is no temperature gradient in optomechanical housing and
detector.
'3-) Optical transmission is assumed to be equivalent to the transmission
calculated at the wavelength defined by the constant "wave" in the code.
,
'Optical setup constructed in FRED must be compliant with the following
items:
,
'1-) Source must be created with an entity name "Source", a power value
calculated according to radiation cone angle which covers the whole cold stop
at the maximum detector pixel position from the optical axis, a single
wavelength equivalent to the constant "wave" defined in code, and a
sufficient number of rays depending on the precision of the calculation
needed.
'2-) Each optical surface in the design must have a suitable optical coating
and "Allow all" raytrace property.
'3-) Emissivities and temperatures must be assigned to all of the radiating
optomechanical surface under the "Auxiliary Data" tab with name "temp" for
temperatures and "emiss" for emissivities.
'4-) An absorbing optical surface covering the optical aperture must be
created in front of the optical system with a description "environment" and a
traceability status off.
'5-) An absorbing surface must be created at the detector FPA position with a
description "FPA"
'6-) A perfect transmitting surface must be created with a description "cold
stop aperture" with a diameter value equivalent to the cold stop aperture
diameter value at the exact position of the cold stop.
,
'Code parameters:
,
'1- wav1: lower limit of operating wavelength (in um)
'2- wave: wavelength at which optical transmission is calculated (in um)
'3- wav2: upper limit of operating wavelength (in um)
'4- PixSize: detector pixel size (in mm)
'5- PixNumX: detector pixel number in x direction
```

```

'6- PixNumY: detector pixel number in y direction
'7- SceneTemp: Scene temperature (in K)
'8- IterNumX: calculation sample in +x direction
'9- IterNumY: calculation sample in +y direction
,
'Outputs:
,
'1- 3D Total NITD vs Detector pixel positions as an ARN
'2- 3D NITD (offset corrected) vs Detector pixel positions as an ARN
'3- 3D TSE vs Detector pixel positions as an ARN
'4- NITD.fgd: NITD values are stored in 2D array format
'5- NITD_offset.fgd: NITD_offset values are stored in 2D array format
'6- TSE.fgd: TSE values are stored in 2D array format
,
'Author : Serhat Hasan ASLAN
'Company: ASELSAN - MGEO
'Contact: shaslan@aselsan.com.tr

'#Language "WWB-COM"

Option Explicit

Const sbConst = 5.670323*10^-12 'Stefan-Boltzmann constant (W/cm^2/K^4)
Const Clight= 3*10^10 'speed of light (cm/s)
Const planck = 6.626*10^-34 'planck constant (J.s)
Const boltzmann = 1.381*10^-23 'Boltzmann constant (W.s/K)

Const wav1 = 3.6
Const wave = 4.2
Const wav2 = 4.9
Const PixSize = 0.015
Const PixArea = PixSize^2
Const PixNumX = 640
Const PixNumY = 512
Const SceneTemp = 300

Sub Main

    Dim NarcSurfList() As Integer, i As Integer, j As Integer, k As Integer,
m As Integer, HousingSurfList() As Integer, IterNum As Integer, SourceNode As
Integer, OpIndex As Integer
    Dim EmissList() As Double, TempList() As Double, frac As Double, emiss
As Double, temp As Double, SumIntTempDerivOfPlanck As Double, ColdStopApNode
As Double, CSgcf As Double, IterStep As Double, ShiftVal As Double, TSE_max
As Double, NITD_min As Double, NITD_max As Double, DetSizeX As Double,
DetSizeY As Double, IterstepX As Double, IterstepY As Double, OpticTrans As
Double

    Dim ResultFileName As String

    Dim NITD_arn As Long, NITD_offset_arn As Long, TSE_arn As Long, IterNumX
As Long, IterNumY As Long

    Dim adv As T_ADVANCEDRAYTRACE
    Dim op As T_OPERATION

```





```

& "TSE(W) " & "      " & "NITD_offset(K) "

    For k=1 To 2*IterNumY+1
        For i=1 To 2*IterNumX+1
            Print DetPosX(i-1) & "      " & DetPosY(k-1) & "      "& NITD(i-
1,k-1) & "      " & TSE(i-1,k-1) & "      " & NITD_offset(i-1,k-1)
        Next
    Next

    NITD_arn = ARNCreate2DGrid("NITD",2*IterNumX+1,-(DetSizeX+IterstepX)/2
,(DetSizeX+IterstepX)/2,2*IterNumY+1,-
(DetSizeY+IterstepY)/2,(DetSizeY+IterstepY)/2,"Double")
    ARNSetDataAsDoubleArray NITD_arn, NITD
    ARNSetAAxisParams NITD_arn, "X pixel Position", GetUnits(), "Spatial"
    ARNSetBAxisParams NITD_arn, "Y pixel Position", GetUnits(), "Spatial"
    ARNSetTitle NITD_arn, "NITD"
    ARNSetDataUnits NITD_arn, "Kelvin"
    ARNAppendToInfo NITD_arn, "Narcissus induced temperature difference(NITD)
at the detector"
    ARNWriteToFile( NITD_arn, GetDocDir() & "\NITD.fgd", False, False )

    NITD_offset_arn = ARNCreate2DGrid("NITD offset",2*IterNumX+1,-
(DetSizeX+IterstepX)/2 ,(DetSizeX+IterstepX)/2,2*IterNumY+1,-
(DetSizeY+IterstepY)/2,(DetSizeY+IterstepY)/2,"Double")
    ARNSetDataAsDoubleArray NITD_offset_arn, NITD_offset
    ARNSetAAxisParams NITD_offset_arn, "X pixel Position", GetUnits(),
"Spatial"
    ARNSetBAxisParams NITD_offset_arn, "Y pixel Position", GetUnits(),
"Spatial"
    ARNSetTitle NITD_offset_arn, "NITD offset"
    ARNSetDataUnits NITD_offset_arn, "Kelvin"
    ARNAppendToInfo NITD_offset_arn, "Narcissus induced temperature
difference(NITD) (DC term corrected) at the detector"
    ARNWriteToFile( NITD_offset_arn, GetDocDir() & "\NITD_offset.fgd", False,
False )

    TSE_arn = ARNCreate2DGrid("TSE",2*IterNumX+1,-(DetSizeX+IterstepX)/2
,(DetSizeX+IterstepX)/2,2*IterNumY+1,-
(DetSizeY+IterstepY)/2,(DetSizeY+IterstepY)/2,"Double")
    ARNSetDataAsDoubleArray TSE_arn, TSE
    ARNSetAAxisParams TSE_arn, "X pixel Position", GetUnits(), "Spatial"
    ARNSetBAxisParams TSE_arn, "Y pixel Position", GetUnits(), "Spatial"
    ARNSetTitle TSE_arn, "TSE"
    ARNSetDataUnits TSE_arn, "Watts"
    ARNAppendToInfo TSE_arn, "Thermal self emission at the detector"
    ARNWriteToFile( TSE_arn, GetDocDir() & "\TSE.fgd", False, False )

    SetTextFileOff
    SetTraceable SourceNode, False
    Update

    Print "Finished!"

End Sub

Sub GetNarcSurfList (ByRef NarcSurfList)

    Dim count As Integer, i As Long
    Dim rtctrl As Long

```

```

ReDim NarcSurfList(0)

NarcSurfList(0) = -1
count = GetEntityCount()
  For i = 1 To count

    If IsSurface(i) Then
      rtctrl = GetSurfRaytraceCtrl(i)
      If rtctrl <>0 Then

        If NarcSurfList(0) = -1 Then
          NarcSurfList(0) = i
        Else
          ReDim Preserve NarcSurfList(UBound(NarcSurfList,1)+1)
          NarcSurfList(UBound(NarcSurfList,1)) = i
        End If
      End If
    End If
  Next

End Sub

Sub GetHousingSurfList(ByRef HousingSurfList,ByRef EmissList, ByRef TempList,
ByRef ColdStopApNode)

  Dim count As Integer, i As Long
  Dim EmissVal As Double, TempVal As Double
  Dim rtctrl As Long
  Dim descript As String
  ReDim HousingSurfList(0)
  ReDim EmissList(0)
  ReDim TempList(0)

  HousingSurfList(0) = -1
  count = GetEntityCount()
  For i = 1 To count

    If IsSurface(i) Then

      descript = GetDescription(i)
      If descript = "cold stop aperture" Then
        ColdStopApNode = i
      End If

      rtctrl = GetSurfRaytraceCtrl(i)
      If rtctrl =0 Then

        If HousingSurfList(0) = -1 Then

          HousingSurfList(0) = i

        Else

          ReDim Preserve
HousingSurfList(UBound(HousingSurfList,1)+1)
          HousingSurfList(UBound(HousingSurfList,1)) = i

          ReDim Preserve EmissList(UBound(EmissList,1)+1)
          ReDim Preserve TempList(UBound(TempList,1)+1)
        End If
      End If
    End If
  Next
End Sub

```



```

                End If
            End If
        End If

        Next

    End Sub

Sub IntTempDerivOfPlanck(ByRef SumIntTempDerivOfPlanck As Double)

    Dim i As Integer
    ReDim DerivPlanck(0) As Double
    Dim StepSize As Double, BinNum As Double, wav As Double
    StepSize = 0.01
    BinNum = (wav2-wav1)/StepSize+1

    For i=1 To BinNum

        wav = wav1+ (i-1) * StepSize
        DerivPlanck(i-1) = 2 * planck^2 * Clight^3 / (wav/10000)^6 /
boltzmann / SceneTemp^2/( Exp(planck*Clight/(wav/10000)/boltzmann/SceneTemp)-
1)^2 / 10000 * Exp(planck*Clight/(wav/10000)/boltzmann/SceneTemp)
        ReDim Preserve DerivPlanck(UBound(DerivPlanck,1)+1)
        'Print DerivPlanck(i-1) & " " & wav

    Next

    SumIntTempDerivOfPlanck = 0

    For i=1 To BinNum-1
        SumIntTempDerivOfPlanck = SumIntTempDerivOfPlanck + (DerivPlanck(i-
1)+DerivPlanck(i))/2*StepSize
    Next

    'Print SumIntTempDerivOfPlanck

End Sub

Sub OpticalTransmission(ByRef OpticTrans As Double)

    Dim tEnt As T_ENTITY
    Dim adv As T_ADVANCEDRAYTRACE
    Dim spNode As Long, refNode As Long, envNode As Long,i As Long
    Dim descr As String

    For i=1 To GetEntityCount()
        If IsSurface(i) Then
            descr = GetDescription(i)

            If descr = "FPA" Then
                refNode = i
                Print refNode

            ElseIf descr = "environment" Then
                envNode =i
                Print envNode
            End If
        End If
    Next
End Sub

```

```

End If

If IsSource(i) Then
    SetTraceable i, False
End If
Next

InitEntity tEnt
tEnt.name = "SourceOpticTrans"
tEnt.description = "Source created for calculation of optical
transmission"
spNode = AddSourcePrim( "Plane Wave (incoherent)", tEnt )
SourcePrimSetParmValue(spNode,0,1)
SourcePrimSetParmValue(spNode,1,1)
SourcePrimSetParmValue(spNode,2,0.001)
SourcePrimSetParmValue(spNode,3,0.001)
SourcePrimSetParmValue(spNode,4,"Rectangle/Square")
SourcePrimSetParmValue(spNode,5,"0, 0, 1.0")
SourcePrimSetWavelSpectValue( spNode, "Single")
SourcePrimSetWavelSingle(spNode,wave)
SourcePrimSetDrawColor( spNode, 255, 0, 0 )
Update

RestartCoordSys spNode,refNode
SetTraceable envNode, True

InitAdvancedRaytrace adv
adv.draw = False
adv.rayPaths = True
adv.drawEveryNthTracedRay = False
AdvancedRaytrace ( adv )
OpticTrans = GetSurfAbsorbedPower ( envNode )
' Print "Optical transmission is:" & OpticTrans
SetTraceable spNode, False
SetTraceable envNode, False
Update

End Sub

```

## CURRICULUM VITAE

### PERSONAL INFORMATION

**Surname, Name:** Aslan, Serhat Hasan  
**Nationality:** Turkish (TC)  
**Date and Place of Birth:** 22.07.1984, Denizli  
**Work Experience:** ASELSAN-MGEO(2008-Present)  
**E-mail address:** shaaslan@gmail.com / shaslan@aselsan.com.tr

### EDUCATION

Degree	Institution	Year of Graduation
Ph.D.	METU Physics	2022
M.S.	METU Physics	2016
B.S.	METU Electrical and Electronics Engineering	2007

### COMPUTER SKILLS

ZEMAX Optical Design Software	Advanced
CODEV Optical Design Software	Advanced
FRED Straylight Analysis Software	Advanced
MATLAB	Advanced

### PUBLICATIONS

1. S. H. Aslan and S. K. Yerli, "Thin lens narcissus model in infrared lens design with cooled detectors," Appl. Opt., vol. 61, no. 3, pp. 728–736, Jan 2022.

## CERTIFICATES

Optical Design Using ZEMAX	ZEMAX
SC159 Head-Mounted Displays: Design and Applications	SPIE
SC154 Electro-Optical Imaging System Performance	SPIE
Course in Sequential /Non-Sequential Analysis Using ZEMAX	ZEMAX
GÖKTÜRK Earth Observation Satellite Project: Introduction Training	Thales Alenia Space
GÖKTÜRK Earth Observation Satellite Project: Advanced Training	Thales Alenia Space
CODEV Software Training Modern Optical Engineering	Optical Research Associates Light Tec. The Institute of Optics, University of Rochester
Optical System Design	The Institute of Optics, University of Rochester
FRED Optical Engineering Software Tutorial	Photon Engineering
FRED Scripting Tutorial	Photon Engineering
Principles of Straylight Short Course	Photon Engineering
Applied Optics	Imperial College of London
Zemax Optical System Design	ZEMAX
Physical Optics Modelling with FRED	Photon Engineering